Titre: Title:	Analysis of Load-Flow Solution Methods for AC/DC Distribution Systems
Auteur: Author:	Amir Mohammad Sadati
Date:	2020
Type:	Mémoire ou thèse / Dissertation or Thesis
Référence: Citation:	Sadati, A. M. (2020). Analysis of Load-Flow Solution Methods for AC/DC Distribution Systems [Mémoire de maîtrise, Polytechnique Montréal]. PolyPublie. https://publications.polymtl.ca/5227/

URL de PolyPublie: PolyPublie URL:	https://publications.polymtl.ca/5227/
Directeurs de recherche: Advisors:	Jean Mahseredjian, & Keyhan Sheshyekani
Programme: Program:	génie électrique

POLYTECHNIQUE MONTRÉAL

affiliée à l'Université de Montréal

Analysis of Load-Flow Solution Methods for AC/DC Distribution Systems

AMIR MOHAMMAD SADATI

Département de Génie Électrique

Mémoire présenté en vue de l'obtention du diplôme de Maîtrise ès sciences appliquées

Génie Électrique

Avril 2020

POLYTECHNIQUE MONTRÉAL

affiliée à l'Université de Montréal

Ce mémoire intitulé:

Analysis of Load-Flow Solution Methods for AC/DC Distribution Systems

présenté par **Amir Mohammad SADATI**

en vue de l'obtention du diplôme de Maîtrise ès sciences appliquées

a été dûment accepté par le jury d'examen constitué de :

Houshang KARIMI, président
Jean MAHSEREDJIAN, membre et directeur de recherche
Keyhan SHESHYEKANI, membre et codirecteur de recherche
Omar SAAD, membre

DEDICATION

To my wife, Maryam, my parents, and my sister for their love, endless support, and encouragement…

ACKNOWLEDGEMENTS

I would like to express my deepest gratitude to my supervisor, Professor Jean Mahseredjian for his continuous support, valuable advice, and encouragement during my research. His outstanding guidance was crucial for the completeness of this thesis.

My appreciation is also extended to my co-supervisor and other jury members for their valuable comments on my thesis.

I would also like to thank my friends at Polytechnique Montreal, whose valuable discussions and support helped me throughout my research.

Finally, I wish to express my deepest gratitude to my wife, Maryam, for her endless love, patience, understanding, and support during my studies. Also, I would like to thank my parents and my sister for their continuous encouragement, patience, support, and prayers.

RÉSUMÉ

Les systèmes de distribution CA/CC ont récemment reçu plus d'attention car ils sont capables de fonctionner à la fois en mode connecté au réseau et en mode isolé. Comparés aux systèmes de distribution CA conventionnels, ils offrent une intégration plus pratique des composants à base de CC tels que les sources d'énergie renouvelables, les systèmes de stockage et les véhicules électriques. Plusieurs travaux de recherche ont porté sur l'analyse d'écoulement de puissance des systèmes d'alimentation CA/CC à différents niveaux de tension. Cette analyse comprend l'analyse d'écoulement de puissance CA/CC pour les systèmes à courant continu haute tension (CCHT), moyenne et basse tension des réseaux de distribution CA/CC et microréseaux dans les deux modes de fonctionnement connectés au reseau et en îloté.

L'objectif de ce projet de recherche est d'examiner en détail les méthodes d'écoulement de puissance CA/CC en fonction de leurs approches de modélisation de système et de leurs procédures de solution. De plus, cette thèse valide deux méthodes d'écoulement de puissance récemment proposées pour les systèmes de distribution CA/CC avec différentes approches de modélisation et manières de solution en utilisant un logiciel de simulation de domaine temporel (EMTP). Suivi de la validation, les méthodes d'écoulement de puissance CA/CC sont comparées entre elles en termes de performances. Enfin, deux techniques d'amélioration sont proposées et appliquées à ces méthodes d'écoulement de puissance pour améliorer leurs performances.

ABSTRACT

AC/DC distribution systems have recently received more attention as they are able to operate in both grid-connected and isolated modes. Compared to conventional AC distribution systems, they offer more convenient integration of DC-based components such as renewable energy sources, storage systems, and electric vehicles. Several research works have been dealt with load-flow analysis of AC/DC power systems at different voltage levels. This includes AC/DC load-flow analysis for high voltage direct current (HVDC) systems, medium and low voltage AC/DC distribution systems and microgrids in both grid-connected and islanded modes of operation.

The objective of this research project is to comprehensively review AC/DC load-flow methods based on their system modeling approaches and solution procedures. Moreover, this thesis validates two recently proposed load-flow methods for AC/DC distribution systems with different modeling approaches and solution manners utilizing a time-domain simulation software (i.e. EMTP). Followed by the validation, the AC/DC load-flow methods are compared to each other in terms of their performances. Finally, two improvement techniques are proposed and applied into those AC/DC load-flow methods to enhance their performances.

TABLE OF CONTENTS

LIST OF TABLES

LIST OF FIGURES

LIST OF SYMBOLS AND ABBREVIATIONS

AC	Alternating Current
DC	Direct Current
DG	Distributed Generator
HVDC	High-Voltage Direct Current
IGBT	Insulated-Gate Bipolar Transistor
LV	Low-Voltage
MANA	Modified Augmented Nodal Analysis
MV	Medium-Voltage
PCC	Point of Common Coupling
p.u.	Per Unit
PV	Photovoltaics
PWM	Pulse Width Modulation
VSC	Voltage Source Converter

LIST OF APPENDICES

CHAPTER 1 INTRODUCTION

1.1 Context

Due to a considerable growth in utilizing DC-based distributed generators (e.g. PV) [1] and energy storage systems (e.g. batteries) [2] in recent years, and also high demand of DC power to supply DC loads (e.g. electric vehicles) in near future [3], conventional AC power systems must change to AC/DC systems which includes both AC and DC buses and lines, and also AC/DC converters working as the interface between AC and DC parts [4]. Therefore, various AC/DC distribution systems have been recently proposed in the literatures [5].

AC/DC distribution systems reduce the overall number of power conversion stages (resulting in loss reduction) [6, 7] and facilitate the integration of renewable energy sources and storage systems [4]. They consist of AC and DC distributed generators (DGs) and energy storage systems which can supply the local loads, and interlinking AC/DC converters that can control the power flows between AC and DC subgrids [8]. Hence, in case a fault occurs in the utility grid or in remote areas where there is no connection between the AC/DC distribution systems and the main grid, they can operate autonomously (i.e. islanded mode).

However, the presence of power electronic devices in different components of AC/DC distribution systems such as DC-based DGs, power converters, storage systems, and DC loads, results in more complicated planning, operation, and time-domain initialization of such systems which need to be addressed by precise analyses.

Load-flow analysis is the most significant and essential approach to deal with the complexities in power system planning and operation [9]. In addition to the establishment of operating conditions, the load-flow solution allows initializing time-domain simulations [10]. Hence, an accurate load-flow computation method is necessary for the planning, operation, and time-domain simulation of various types of power systems. An accurate load-flow analysis can be obtained by precise modeling of the system. For AC/DC distribution systems, this model must include the AC and DC subgrids of the system as well as the converter models along with their control schemes. Moreover, the load-flow solution for such systems must be capable of performance under islanded mode of operation in which the frequency is not constant and it is one of the load-flow problem variables.

Several load-flow methods have been proposed for AC/DC distribution systems in both grid-connected and islanded modes of operation. In this research project, these load-flow methods are reviewed based on their system modeling approach and solution procedure. Moreover, two recent load-flow methods for AC/DC distribution systems are validated using a time-domain simulation software (i.e. EMTP) and then compared to each other with respect to efficiency of the solution algorithm. Finally, two techniques are proposed to improve the efficiency of these AC/DC load-flow algorithms.

1.2 Research Objectives

The objectives of this research project are as follows:

- Comprehensive review of published load-flow solution methods for AC/DC power systems.
- Validating selected AC/DC load-flow methods proposed in the literature using a time-domain simulation software and comparison of those methods in terms of efficiency.
- Improving of efficiency of selected load-flow algorithms for AC/DC distribution systems.

1.3 Thesis Outline

This thesis is organized as follows:

In Chapter 2, previous research on published load-flow methods for AC/DC distribution power systems are presented.

In Chapter 3, a comprehensive review on load-flow methods for grid-connected and islanded AC/DC distribution systems is presented. This includes different solution methods and models.

In Chapter 4, two recently proposed AC/DC load-flow methods based on decoupled and unified approaches are validated by comparing their results with a time-domain simulation tool (i.e. EMTP). Furthermore, their performances are compared to each other and two improvement techniques are introduced to increase their efficiencies.

Finally, Chapter 5 summarizes the work presented in this thesis and suggests directions for future research work.

CHAPTER 2 LITERATURE REVIEW

In this chapter, previous research on load-flow analysis of AC/DC power systems are presented. Section 2.1 represents a brief description of different AC/DC power systems and their components. Section 2.2 reviews the AC/DC load-flow methods proposed in the literature for different types of AC/DC power systems.

2.1 AC/DC Power Systems

AC technology was introduced as the standard for power generation, transmission and distribution due to the convenient transformation of the voltage level via AC transformers. These transformers could easily step up the generated medium voltage to high voltage to be used in transmission lines and step down the high voltage to medium and low voltage to be used in distribution systems.

At transmission level, there are several limitations for high voltage AC technology such as transmission capacity, distance restriction, and direct connection of two networks with different frequencies [11]. To address these limitations, high-voltage direct current (HVDC) power systems have been introduced.

At distribution level, the gradual conversion in load types from AC to DC, and the appearance of renewable energy-based DGs necessitate numerous power conversion in AC systems which results in lower efficiency [4]. Therefore, DC distribution systems have been proposed to integrate DC-based DGs and feed the DC loads with reduced number of power conversion [12]. However, in DC distribution systems, AC power sources have to be inverted to DC and the conventional AC loads require DC/AC converters [12]. Hence, hybrid AC/DC distribution systems have been proposed to eliminate the unnecessary AC/DC and DC/AC power conversions [7]. These systems can also exist in form of AC/DC microgrids. In general, AC/DC microgrid refers to a low- or medium-voltage hybrid power system in which the components are grouped into an AC grid, a DC grid, and an interlinking converter which is a power electronics interface that enables power exchange between AC and DC grids [4, 13]. These hybrid systems are usually able to operate in both grid-connected and islanded conditions. The structure of a medium-voltage (MV) AC/DC distribution system which is connected to high-voltage AC and DC systems via transformers and power converters is illustrated in Figure 2.1. In this system, both AC and DC grids consist of DG units (e.g. PV, wind

turbine, diesel generator, and fuel cell), energy storage systems (e.g. batteries), AC and DC loads, and power converters (e.g. DC/DC and AC/DC).

AC/DC microgrids or in more generic terms, AC/DC distribution systems decrease the overall AC/DC power conversions which results in cost and loss reduction [14, 15]. Moreover, these systems offer a convenient and smooth integration of renewable energy sources [16, 17], energy storage systems [2], and electric vehicles [18, 19]. However, due to the intermittent nature of renewable energy sources [20] and highly stochastic nature of some of the loads such as electric vehicles [21], integration issues such as complex control schemes must be addressed in various studies such as load-flow analysis in AC/DC distribution systems [4, 22].

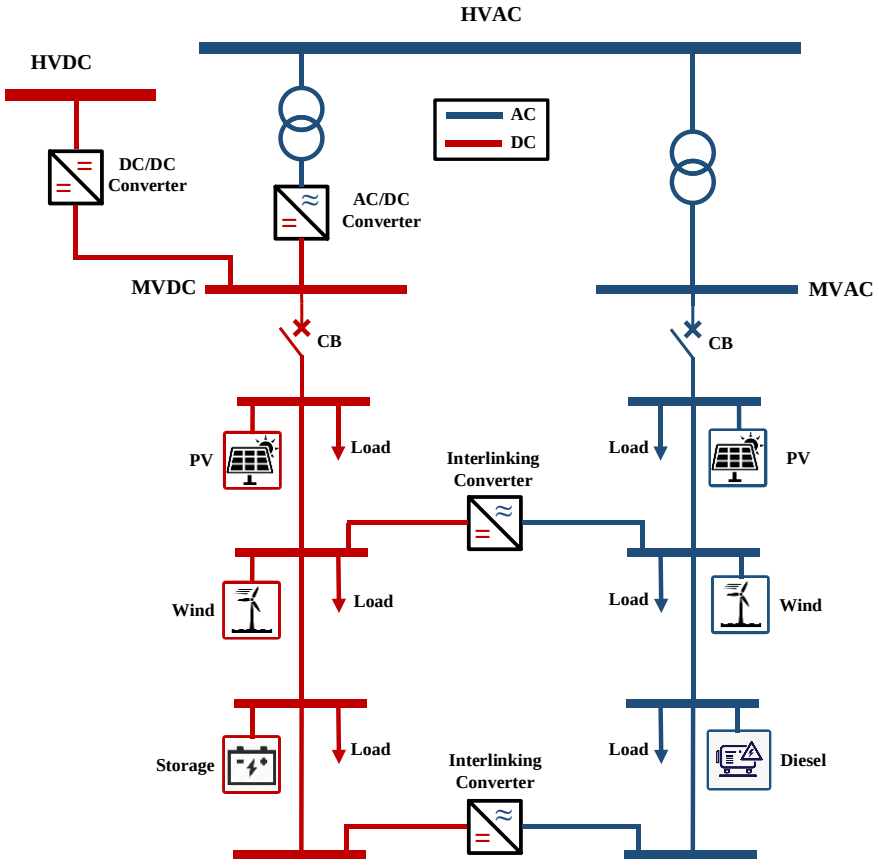

Figure 2.1 Structure of AC/DC distribution system

2.2 Load-Flow Analysis in AC/DC Power Systems

The load-flow analysis is a numerical study to calculate the steady-state flow of electric power in a power system. The main outputs of this study are voltage magnitudes and phase angles of all the buses in system. Load-flow is a fundamental analysis method in power system studies, such as planning, economical scheduling, system operating and control [9]. In addition to investigation of power systems in their steady-state [23], load-flow analysis can provide initialization means for time-domain simulations [10].

Since AC system has been the most commonly used technology in power systems, the majority of research work on load-flow analysis devoted to such systems. In the load-flow study of AC power systems, each bus has four parameters (voltage magnitude, phase angle, active power, and reactive power) taken part in the analysis. The goal of load-flow analysis is to calculate unknown parameters for each bus. Typically, the AC load-flow problem is formed using conventional nodal analysis [24]. However, other formulation approaches such as modified augmented nodal analysis (MANA) [25] or augmented rectangular [26] have been proposed. MANA formulation of the system equations is achieved by augmenting additional devices equations to the conventional nodal equations. It results in a generic multiphase load-flow formulation that can include arbitrary system topologies, and can be extended to accommodate various component models and it provides a precise initialization for a time-domain simulation tool (EMTP) [10, 25].

Traditionally, load-flow was solely performed for AC power systems. However, due to the utilization of HVDC systems, AC/DC load-flow has been investigated since 1970s [27, 28]. The existing AC/DC load-flow methods in the literatures have been proposed for AC/DC power systems at different voltage levels such as HVDC transmission systems [29-33], medium-voltage (MV) and low-voltage (LV) AC/DC distribution systems [34-36] or hybrid AC/DC microgrids in both grid-connected and islanded modes of operation [37-41]. These methods usually utilize the decoupled modeling approach in which the AC/DC power system is divided into three parts, AC grid, DC grid, and interlinking converter and then each of these parts are modeled separately. AC/DC power systems can also be modeled as a unified system for the load-flow analysis [34].

Generally, AC/DC load-flow solution methods are categorized into two types, the sequential method and the unified method. The sequential method was proposed by [28] and it solves load-

flow equations of AC and DC systems sequentially in each iteration of the solution. In contrast, the unified method, proposed by [27], solves the load-flow equations of AC and DC systems simultaneously.

In sequential AC/DC load-flow solution approach, the three sets of system equations (i.e. AC grid, DC grid, and interlinking converter) are solved separately. This method usually starts with estimation of DC system parameters. Afterwards, it finds the AC system equations solution and used it to modify the estimated DC parameters. After this modification, the whole AC system solution must be repeated. This iterative process continues until convergence is obtained [29]. The main advantage of the sequential method is that it requires lower computational requirements as it can be coded in existing load-flow analysis programs [42]. However, due to the additional iterative loops, the sequential method is more time consuming and it may have convergence problems in case one of the internal loops does not converge [43-45]. Several algorithms mostly based on the Newton iterative method have been proposed for the sequential load-flow analysis of AC/DC power systems [29, 32, 35, 39, 44, 46-49]. In addition to Newton-based algorithms in sequential approach, branched-based algorithms can also be employed to solve load-flow problem in AC/DC power systems [50].

In unified load-flow method, all sets of AC/DC power system's equations are solved simultaneously. In contrast with the sequential method, the unified method has less computation time with higher accuracy, as it does not consider any assumptions in simplifying the relationship between AC and DC grids [51]. Moreover, unified method has more robust convergence feature as only one set of equations is solved in this method [52]. However, implementing the unified method is more complicated than the sequential method as the existing load-flow programs are still not well developed for this kind of approach [53]. Similar to the sequential approach, the most commonly employed algorithms to solve the AC/DC load-flow problems with unified approach are also based on Newton iterative method [30, 33, 38, 51, 52, 54].

Several studies have been carried out on comparison of different AC/DC load-flow methods and solution procedures, and their advantages and disadvantages have been discussed [55-57].

CHAPTER 3 LOAD-FLOW METHODS FOR AC/DC DISTRIBUTION SYSTEMS

In this chapter, a comprehensive review on load-flow methods for grid-connected and islanded AC/DC distribution systems is presented. Section 3.1 introduces decoupled and unified modeling approaches for load-flow analysis of AC/DC distribution systems. Section 3.2 presents AC/DC load-flow problem formulation and solution methods based on each modeling approaches.

3.1 Modeling of AC/DC Distribution Systems for Load-Flow Analysis

Modeling of the power system is one of the most significant steps for load-flow analysis. The more accurate the modeling is performed for a power system; the more precise load-flow results can be obtained. As mentioned before, there are two main modeling approaches for load-flow analysis of AC/DC distribution systems, the decoupled and the unified. These approaches are presented in detail in the following.

3.1.1 Decoupled Modeling

In this modeling approach, the AC/DC distribution system is divided into three sections, the AC grid, the DC grid, and the AC/DC interlinking converter, and these sections are modeled separately.

3.1.1.1 AC Grid Modeling

Plenty of research have been carried out on modeling of AC grids for the conventional load-flow studies of AC power systems [9, 58]. For load-flow analysis, an AC grid is represented by number of buses (nodes) with generators and loads connected to them. Moreover, these buses can be connected to each other via connection lines. The load-flow problem is defined for each bus (e.g. bus "i") in terms of its complex voltage ($V_i \angle \delta_i$) and apparent injected power ($S_i = P_i + jQ_i$). In general, there are three types of buses in conventional grid-connected AC grids, slack bus, AC load bus (or PQ), and AC voltage-controlled bus (or PV). Slack buses have fixed reference voltage magnitude and phase angle. In PQ buses, active and reactive powers are known, and PV buses have fixed voltage magnitude and active power. Another required parameter for the load-flow solution

is the admittance matrix (***Y***) which represents the nodal admittance of the buses [59]. The generic load-flow equations for bus "i" in an AC grid are as follows [9]:

$$P_i = V_i \sum_{j=1}^{N_{ac}} Y_{ij} V_j \cos(\delta_i - \delta_j - \theta_{ij}) \tag{3.1}$$

$$Q_i = V_i \sum_{j=1}^{N_{ac}} Y_{ij} V_j \sin(\delta_i - \delta_j - \theta_{ij}) \tag{3.2}$$

where, P_i and Q_i are the injected active and reactive powers at bus "i", N_{ac} is the number of AC buses, V_i and δ_i are magnitude and phase angle of the voltage at bus "i", and Y_{ij} and θ_{ij} are admittance between buses "i" and "j" and its angle, respectively.

In case of AC/DC power systems, there are some other approaches for modeling the AC grid to obtain the load-flow equations. For instance, an extended AC grid model including the elements connected between the point of common coupling (PCC) and the AC bus of the AC/DC converter has been proposed (Figure 3.1) [33, 46]. These elements are coupling transformers, low-pass filters and line reactors and they are included in admittance matrix for the load-flow equations of the AC grid.

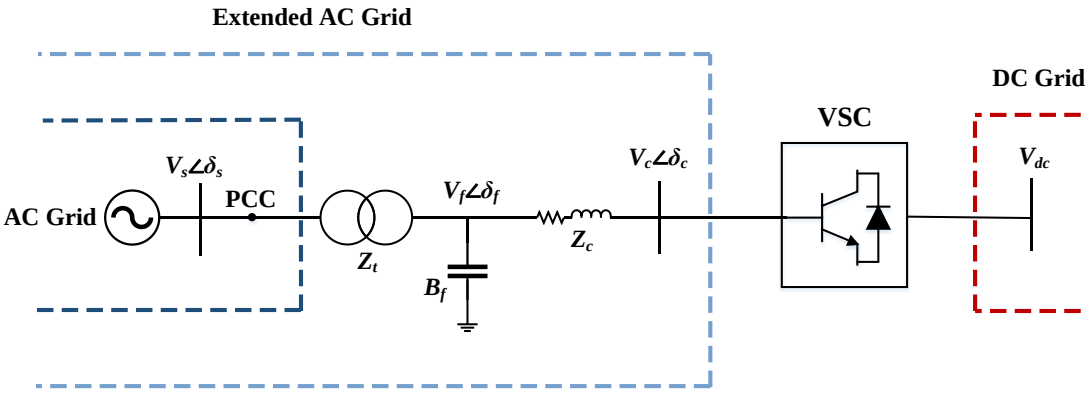

Figure 3.1 Extended AC grid model [33]

In isolated cases (e.g. islanded microgrids), due to the lack of a stiff AC grid, the AC system's frequency is not constant anymore and it may vary. Therefore, the admittance terms which are function of the system's frequency ($Y(\omega)$) will change with variation in frequency [39, 60]. In

addition to considering the frequency change in the admittance matrix, it is necessary to obtain a frequency dependent model for loads [37, 61]. Moreover, in islanded cases, since DGs may operate in droop mode, it is required to obtain droop-based models for DGs [37, 62, 63] and storage systems [64, 65].

In the following, modeling procedure of AC loads and DGs for load-flow analysis are explained, respectively.

AC loads can be represented by the composite load model which includes both static and dynamic characteristics of the load. Static load model represents the active and reactive powers at any time as functions of bus voltage magnitude and frequency at that time, respectively [61]. For load-flow analysis which is a steady-state study, static load model is commonly used [66].

The exponential static load model considering the impact of voltage is represented as [39]:

$$P_L = P_{L,0}(V_{ac})^{\alpha} \tag{3.3}$$

$$Q_L = Q_{L,0}(V_{ac})^{\beta} \tag{3.4}$$

Where, $P_{L,0}$ and $Q_{L,0}$ are nominal active and reactive power, α and β are active and reactive power exponents. Based on the different values of α and β, this model can represent constant impedance ($\alpha = \beta = 2$), constant current ($\alpha = \beta = 1$), or constant power ($\alpha = \beta = 0$) loads. A combination of constant impedance, constant current, and constant power loads can be represented by the ZIP or polynomial load model in which the ZIP coefficients are assigned according to the type of each load. The ZIP model can be presented as [67]:

$$P_L = P_{L_0}\left[Z_p\left(\frac{V_{ac}}{V_{ac_0}}\right)^2 + I_p\left(\frac{V_{ac}}{V_{ac_0}}\right) + P_p\right] \tag{3.5}$$

$$Q_L = Q_{L_0}\left[Z_q\left(\frac{V_{ac}}{V_{ac_0}}\right)^2 + I_q\left(\frac{V_{ac}}{V_{ac_0}}\right) + P_q\right] \tag{3.6}$$

where, P_{L_0} and Q_{L_0} are nominal active and reactive powers, V_{ac_0} is nominal AC voltage, and $Z_{p,q}$, $I_{p,q}$, and $P_{p,q}$ are ZIP coefficients for constant impedance, constant current, and constant power

portions of the load. The sum of ZIP coefficients for each active and reactive power must be equal to 1.

As mentioned before, in islanded cases where the frequency of the system is not constant, an additional term must be added to the load model to consider the frequency dependency of the load [68]. The frequency dependency terms can be added to both exponential and ZIP load model formulas as follows:

$$P_L = P_{L,0}(V_{AC})^{\alpha}(1 + k_{pf}(\omega - \omega_0)) \tag{3.7}$$

$$Q_L = Q_{L,0}(V_{AC})^{\beta}(1 + k_{qf}(\omega - \omega_0)) \tag{3.8}$$

$$P_L = P_{L_0}\left[Z_p\left(\frac{V_{ac}}{V_{ac_0}}\right)^2 + I_p\left(\frac{V_{ac}}{V_{ac_0}}\right) + P_p\right]\left(1 + k_{pf}(\omega - \omega_0)\right) \tag{3.9}$$

$$Q_L = Q_{L_0}\left[Z_q\left(\frac{V_{ac}}{V_{ac_0}}\right)^2 + I_q\left(\frac{V_{ac}}{V_{ac_0}}\right) + P_q\right]\left(1 + k_{qf}(\omega - \omega_0)\right) \tag{3.10}$$

where, ω_0 and ω are the nominal and operating frequencies, respectively, and k_{pf} and k_{qf} are frequency sensitivity parameters.

AC DGs usually operate in PV or PQ control modes in a grid-connected AC grid. However, in islanded cases, they can also operate in droop mode [69]. Similar to the AC buses in load-flow problem, AC DGs can also be associated with four parameters, magnitude and phase angle of the terminal voltage, output active and reactive power. The concept of PV and PQ control of AC DGs is similar to conventional power systems. However, DGs can also be controlled autonomously by their droop characteristics [62]. Based on the droop theory, the frequency and the AC terminal voltage magnitude of droop-based AC DGs are controlled based on local measurements of active and reactive power at each AC bus "i", respectively (Figure 3.2) [63].

$$P_{G_{ac},i} = (\omega_0 - \omega)/\vartheta_{p_{ac}} \tag{3.11}$$

$$Q_{G_{ac},i} = (V_{ac_0,i} - V_{ac,i})/\vartheta_{q_{ac}} \tag{3.12}$$

where ω, ω_0, V_{ac} and V_{ac_0} are operating and nominal frequency and AC terminal voltage magnitude of AC DG, respectively. Moreover, $\vartheta_{p_{ac}}$, $\vartheta_{q_{ac}}$ are the active and reactive power droop gains of the AC DG, respectively, and they can be determined as [34, 39]:

$$\vartheta_{p_{ac},i} = (\omega^{max} - \omega^{min})/P_{G_{ac},i}^{max} \tag{3.13}$$

$$\vartheta_{q_{ac},i} = (V_{ac,i}^{max} - V_{ac,i}^{min})/Q_{G_{ac},i}^{max} \tag{3.14}$$

where, ω^{max} and ω^{min}, $V_{ac,i}^{max}$ and $V_{ac,i}^{min}$ are the maximum and minimum allowed frequency and voltage magnitude of AC grid, respectively. $P_{G_{ac},i}^{max}$ and $Q_{G_{ac},i}^{max}$ are maximum active and reactive powers of AC DG at bus "i".

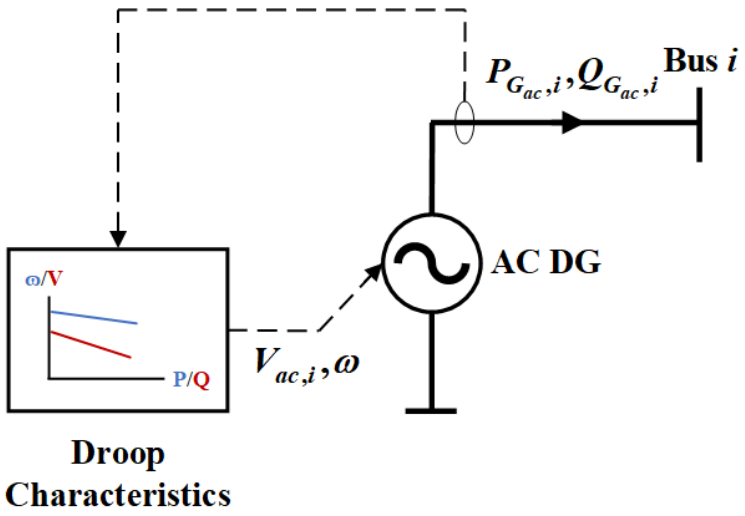

Figure 3.2 Model of AC DG operating in droop mode [69]

In the same manner, droop control can also be employed for AC type storage systems [64, 65].

3.1.1.2 DC Grid Modeling

In comparison with AC grid modeling, DC grid modeling for load-flow analysis has been less investigated due to its more recent applications. Similar to the conventional AC grids, for load-flow analysis, a DC grid is represented by a number of buses with loads and generators connected to them [29]. The load-flow problem is defined for each DC bus in terms of its voltage magnitude and injected active power.

Three types of bus are defined for DC grids:

- DC voltage bus
- DC load bus
- DC droop-based DG bus

In DC voltage-controlled bus and the DC load bus, the voltage magnitude and the injected active power are known, respectively [34]. DC droop-based DG bus is analogous to the AC droop-based DG bus and it is utilized in islanded cases for power sharing among DGs in the DC grid [70]. By employing the droop theory, the DC voltage of the DC DG bus is regulated based on its generated DC power [38].

In DC grids, the active power flow depends on the difference in voltage magnitude between the buses [47]. The injected current of the DC bus "m" can be represented as the current flowing to the other buses in the DC grid [59]:

$$I_{dc,m} = \sum_{\substack{l=1 \\ l \neq m}}^{N_{dc}} G_{dc,ml}(V_{dc,m} - V_{dc,l}) \tag{3.15}$$

where $G_{dc,ml}$ represents the conductance between DC buses "m" and "l". The combined injected currents for a DC grid with "N_{dc}" buses can be written as:

$$\boldsymbol{I_{dc} = G_{dc} V_{dc}} \tag{3.16}$$

where $\boldsymbol{G_{dc}}$ is DC conductance matrix, and $\boldsymbol{V_{dc}}$ is DC voltage vector. The DC active power injected to bus "m" in steady-state is represented by:

$$P_{dc,m} = V_{dc,m} I_{dc,m} \tag{3.17}$$

Substituting (3.15) in (3.17) gives:

$$P_{dc,m} = V_{dc,m} \sum_{\substack{l=1 \\ l \neq m}}^{N_{dc}} G_{dc,ml}(V_{dc,m} - V_{dc,l}) \tag{3.18}$$

In addition to the conventional DC grid modeling, in order to obtain the load-flow equations, there are some other approaches proposed in the literature. In the simplest approach, the DC grid can be modeled as an injected power into the AC grid to which it is connected [29, 59, 71]. This model is usually employed to represent two-terminal HVDC systems [72]. It is appropriate for the studies in which the overall impact of the DC grid on its linked AC grid is more important than the effects of the actual components in that. However, by using this approach, it is not possible to obtain a comprehensive model of DC grid with its components such as DGs, loads, and DC/DC converters [59]. The other modeling approach is to exclude non-linear elements such as DC sources, DC loads, and DC/DC converters, and assume that the DC grid is a linear network for which the conventional modeling approach can be employed [51].

Moreover, in case of line or converter outages, zero current injection feature can be considered for number of buses in DC grid load-flow model [47, 59]. This feature can also be added to the load-flow model by defining a special DC bus category as zero-injection bus [33].

A typical DC grid consists of DGs, loads, and DC/DC converters. DC loads can be modeled as constant power, constant current, or constant resistance loads among which the constant power type is the most frequently used [73, 74]. DC/DC converters, DC motors, and variable speed drives are the typical examples of constant power loads [75]. However, there are some motors that can be modeled as constant current loads due to the almost equal drawn current for wide range of input voltage [39]. Constant resistance loads such as lamps, heaters, and relays can be modeled within the system conductance matrix. Hence, the total load connected to a DC bus can be modeled as [39]:

$$P_{L_{dc},m} = P^0_{dc,m} + V_{dc,m} I^0_{dc,m} \tag{3.19}$$

Where $P^0_{dc,m}$ and $I^0_{dc,m}$ are the load constant power and constant current portions, respectively. This load modeling approach is commonly used for DC loads in AC/DC microgrids [37-39].

In addition to loads, DC grids consist of DC DGs which can operate in constant power or droop modes. Constant power DC DGs can be modeled for load-flow analysis as constant power loads with opposite sign. Droop-based DC DGs can be modeled using DC droop characteristics at each DC bus "m" with the following control structure [38, 39]:

$$P_{G_{dc},m} = (V_{dc_0,m} - V_{dc,m})/\vartheta_{p_{dc},m} \tag{3.20}$$

Where, $P_{G_{dc}}$ is the DG output power, V_{dc_0} is the DG no-load DC reference voltage, and $\vartheta_{p_{dc}}$ is droop gain for DG output power and it can be determined as [34, 39]:

$$\vartheta_{p_{dc},m} = (V_{dc,m}^{max} - V_{dc,m}^{min})/P_{G_{dc},m}^{max} \tag{3.21}$$

Where, $P_{G_{dc},m}^{max}$ is the maximum power of DC DG connected to bus "m", and $V_{dc,m}^{max}$ and $V_{dc,m}^{min}$ are maximum and minimum allowed voltages of DC grid.

In addition to DC DGs and loads, DC grids also consist of DC/DC converters. They are employed to change the DC voltage level like the AC transformers in conventional AC systems [76]. Various topologies with different features have been proposed for DC/DC converters in power applications [77-85]. These converters are mostly based on dual active bridge [77, 85-87], resonant [81, 88], and modular multilevel topologies [83, 84, 89].

In case that the DC grid consists of several DC subgrids which may have different voltage levels, multiport DC/DC converters are required for interconnection of those subgrids. For the DC grids at distribution level, several multiport DC/DC converters have been proposed for integration of renewable DGs [90-92], electric vehicles [93], energy storage systems [94, 95], and photovoltaic systems [96]. At HVDC level, several approaches such as DC hub and DC/DC autotransformer have been proposed for interconnection of multiple DC systems. The DC hub functions as substations in conventional AC systems as it connects multiple DC transmission lines with same or different voltage levels. DC hub's topology is based on multiple IGBT-based AC/DC converters along with an internal LCL circuit [97]. In contrast with DC hub which requires DC/AC/DC conversion, the multiport DC/DC autotransformer utilizes direct electrical connection between the interconnected DC systems [98].

DC/DC converters can be considered as constant power loads in load-flow analysis [74]. However, several load-flow models for these converters have been proposed [49, 85, 99-102]. DC/DC converter topologies can be categorized into two types, non-galvanic (i.e. without isolating transformer) and galvanic isolated (i.e. with isolating transformer) [103]. Boost and bridge converters are the most commonly used non-galvanic and galvanic isolated topologies, respectively [85]. The load-flow model equations considering converter losses and control strategy for a DC/DC converter (Figure 3.3) between two DC buses (m and l), are as follows [85]:

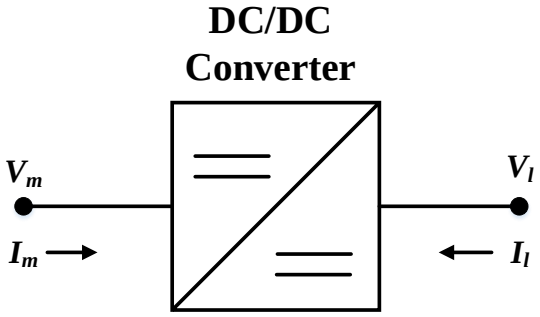

Figure 3.3 DC/DC converter model [85]

$$P_m = \sum_{j \neq l}^{N_{dc}} V_m V_j G_{mj} + V_m I_m \tag{3.22}$$

$$P_l = \sum_{j \neq m}^{N_{dc}} V_l V_j G_{lj} + V_l I_l \tag{3.23}$$

$$V_m I_m + V_l I_l - P_{loss} = 0 \tag{3.24}$$

$$V_m = V_{exp} \tag{3.25}$$

where P_m and P_l are nodal power at bus "m" and "l", G_{xj} (x = m or l) is the element in DC conductance matrix representing the conductance value between bus "m" or "l" and "j". Equation (3.24) is the power balance equation, P_{loss} is the converter losses, and V_{exp} is the expected voltage value at bus "m" Equation (3.25) indicates the control scheme of the converter.

3.1.1.3 AC/DC Interlinking Converter Modeling

In recent years, due to the considerable developments in power electronics technology and the rapid increase in utilization of renewable energy sources which are usually connected to power systems via power electronics converters, AC/DC converters have been comprehensively studied [104]. Among the existing topologies for AC/DC converters, voltage source converters (VSCs) are the most frequently used in power system applications such as generation, transmission, and distribution. VSCs have several advantages compared to line-commutated current source converters [105]. Firstly, as self-commutated topologies, they are able to avoid commutation failures which may happen due to the disturbances in the AC grid. Moreover, they offer independent control for the generated or consumed active and reactive powers of the converter.

VSCs are used as a link between AC and DC grids in AC/DC power systems. Various models of VSCs and their control features have been proposed for AC/DC load-flow analysis at different power system levels. Due to the widespread application of HVDC systems, most of the existing VSC load-flow models have been proposed for these systems. The general representation of the VSC station as an interface between AC and DC grids in an HVDC system is shown in Figure 3.4. VSCs are usually connected to the point of common coupling (PCC) of the AC grid via phase reactors, AC filters and coupling transformers, and at DC side, VSCs are connected to the DC grid via DC capacitors [11]. The phase reactors are employed to regulate the current and consequently control active and reactive power flows [106]. They are also able to reduce the high frequency harmonic of the AC current caused by switching of the VSC [106]. AC filters are used to compensate the impact of high frequency harmonics on output AC voltage [106]. Transformers provide appropriate voltage level for both AC grid and VSC. In addition to voltage ripple reduction, DC capacitors provide storage to facilitate power flow control [106].

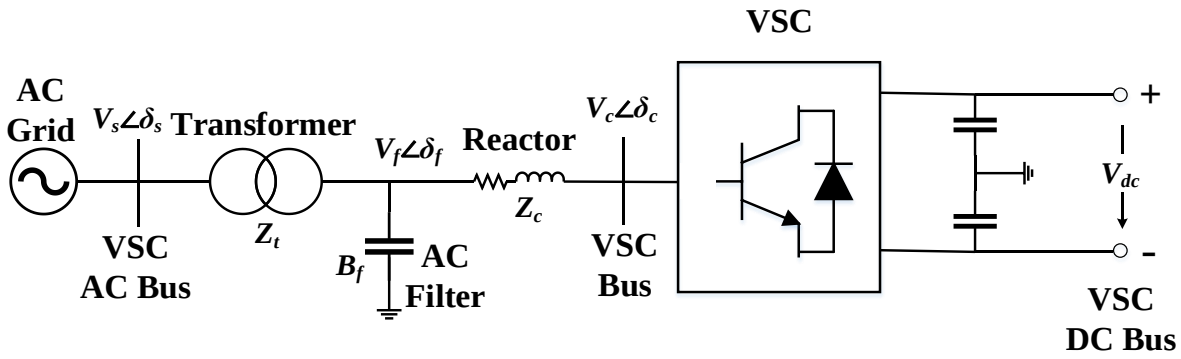

Figure 3.4 Structure of VSC station [42]

In load-flow studies, at the DC side, VSCs are normally represented as controlled current source [35, 54]. At the AC side, they are considered as a controlled voltage source behind a complex admittance (Figure 3.5) consisting of admittances for phase reactor ($Y_c = |Y_c|\angle\theta_c$) and transformer ($Y_t = |Y_t|\angle\theta_t$), and susceptance of AC filter (B_f) [30, 33, 35, 36, 47, 51, 52, 54, 59, 107]. In order to simplify the load-flow model and facilitate the computation of load-flow solution, some of these admittances have been neglected in several investigations [29, 71]. Based on the standard AC load-flow equations (3.1) and (3.2) [9], the injected active and reactive powers to the AC grid (P_s and Q_s) and powers at the AC side of VSC (P_c and Q_c) in terms of complex voltages can be calculated as follows [35]:

$$P_s = -V_s^2|Y_t|\cos\theta_t + V_sV_f|Y_t|\cos(\delta_s - \delta_f - \theta_t) \tag{3.26}$$

$$Q_s = V_s^2|Y_t|\sin\theta_t + V_sV_f|Y_t|\sin(\delta_s - \delta_f - \theta_t) \tag{3.27}$$

$$P_c = V_c^2|Y_c|\cos\theta_c - V_cV_f|Y_c|\cos(\delta_c - \delta_f - \theta_c) \tag{3.28}$$

$$Q_c = -V_c^2|Y_c|\sin\theta_c - V_fV_c|Y_c|\sin(\delta_c - \delta_f - \theta_c) \tag{3.29}$$

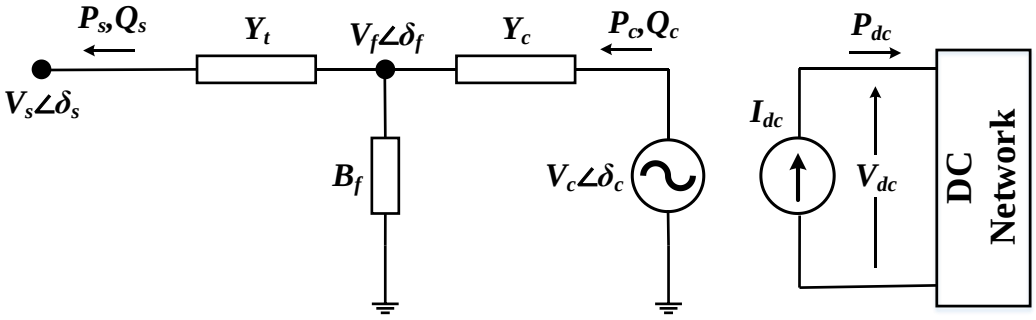

Figure 3.5 VSC station equivalent circuit model [42]

The other equations required for modeling of VSCs in load-flow studies are voltage and active power coupling between AC and DC grid. The terminal voltages at AC (bus "i") and DC (bus "m") sides are coupled by the pulse width modulation (PWM) amplitude index (M) as follows [108, 109]:

$$V_{c,i} = \frac{M}{2\sqrt{2}} V_{dc,m} \tag{3.30}$$

where, "M" is the amplitude modulation index, and $V_{c,i}$ and $V_{dc,m}$ are AC and DC voltages of the VSC, respectively.

The active power at AC and DC sides are also related to each other as [107]:

$$P_c + P_{dc} + P_{loss} = 0 \tag{3.31}$$

Where P_c and P_{dc} are AC and DC power, and P_{loss} is converter loss which will be explained in the following.

In addition to the admittances between VSC and AC grid, converter losses and control modes are the other features which need to be considered in modeling of VSCs for load-flow analysis. A generalized loss model of the VSC must incorporate the AC filter losses, phase reactor losses and the voltage drop in transformer impedance [110]. The overall converter loss can be approximated as a quadratic function of converter current (I_c) which depends on the active and reactive powers exchanged between the VSC and the AC grid as presented in equation (3.32). As shown in equation (3.33), the total converter loss includes constant, linear, and variable components [72]. Constant and linear losses represent no-load and switching losses, respectively. The variable losses which

are associated with square of converter current, include the diode's reverse recovery and generated heat losses [47, 59].

$$I_c = \frac{\sqrt{P_c^2 + Q_c^2}}{V_c} \tag{3.32}$$

$$P_{loss} = A + BI_c + CI_c^2 \tag{3.33}$$

Where, "A", "B", and "C" are the per unit loss coefficients and they can be determined by the test data of converter losses [59]. Converter losses can be neglected in load-flow analysis of low- and medium-voltage AC/DC distribution systems [8, 111]. In this case the AC and DC powers of the converter are equal but opposite in sign. Therefore, in the following sections, converter's power which can present its AC and DC powers is defined as:

$$P_{IC} = P_{dc} = -P_c \tag{3.34}$$

where, IC stands for "interlinking converter".

As mentioned earlier, VSCs are able to control the active and reactive power independently with respect to the AC system. Due to this feature, four control modes have been categorized for VSCs in AC/DC load-flow studies of HVDC systems with respect to active and reactive powers [42]:

- $\boldsymbol{P_{ac}}$**-control:** the VSC controls its constant active power injection P_{ac} into the AC grid.
- $\boldsymbol{V_{dc}}$**-control:** the VSC controls its constant DC voltage V_{dc} by regulating the active power injection P_{ac}.
- $\boldsymbol{Q_{ac}}$**-control:** the VSC controls its constant reactive power injection Q_{ac} into the AC grid.
- $\boldsymbol{V_{ac}}$**-control:** the VSC controls its constant AC bus Voltage V_{AC} by adjusting the reactive power injection Q_{ac}.

In multiterminal HVDC systems, one of the VSCs is modeled as DC slack bus converter to incorporate the DC grid losses and preserve the DC grid voltage. The other VSCs can be considered to operate in PQ or PV control mode in AC grid [42].

In isolated cases like islanded AC/DC microgrids, due to the lack of stiff AC or DC grid, the AC/DC interlinking converter must coordinate AC and DC grids to achieve a specific power sharing objective such as [112]:

- Equal sharing of AC/DC microgrid demand among the DGs based on their ratings
- Equal loading of AC and DC subgrids to prevent overloaded and underloaded conditions

The most commonly used power sharing control strategy for interlinking converters in isolated cases is droop control [70]. As shown in equations (3.11) and (3.20), in droop control theory, ω and V_{dc} can be controlled based on local measurement of active powers in AC and DC subgrids, respectively. Since only active power can be transferred between AC and DC subgrids via interlinking converter, ω and V_{dc} are considered as loading indicators of AC and DC subgrids, respectively. In order to control the active power transfer between two subgrids, they must be compared. Since they have different units, they are normalized in order to be in identical scale and in a range between -1 and 1 [70]:

$$\hat{V}_{dc} = \frac{V_{dc} - 0.5(V_{dc}^{max} + V_{dc}^{min})}{0.5(V_{dc}^{max} - V_{dc}^{min})} \tag{3.35}$$

$$\hat{\omega} = \frac{\omega - 0.5(\omega^{max} + \omega^{min})}{0.5(\omega^{max} - \omega^{min})} \tag{3.36}$$

where, $\hat{V}_{dc}$ and $\hat{\omega}$ are normalized DC terminal voltage and normalized frequency of the AC subgrid, and V_{dc} and ω indicate the DC terminal voltage of the interlinking converter and the frequency of AC subgrid. Superscripts "max" and "min" represent the maximum and minimum allowable value of each variables.

As mentioned above, the active power droop control is an autonomous control scheme as it requires only local measurement of AC subgrid frequency and DC subgrid voltage. Therefore, in order to equalize the loading of AC and DC subgrids, their loading indicators (normalized DC terminal voltage and normalized frequency) must be equalized as follows [70]:

$$\hat{\omega} = \hat{V}_{dc} \tag{3.37}$$

Figure 3.6 illustrates the power sharing process between AC and DC subgrids via interlinking converter using droop control theory.

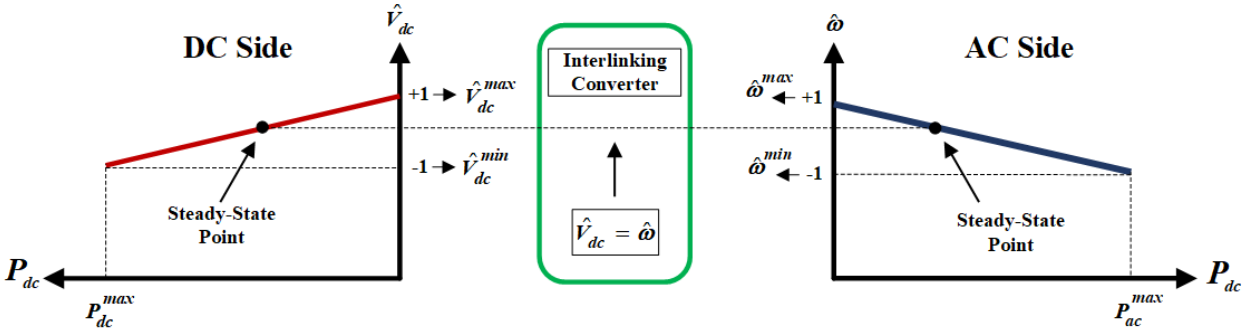

Figure 3.6 Power sharing between AC and DC subgrids using droop control theory [70]

The difference between normalized frequency and DC voltage ($\Delta e = \hat{\omega} - \hat{V}_{dc}$) is an error which should be set to zero by using a control approach in order to have a balanced power sharing between two subgrids [70]. The active power transferred between AC and DC subgrids via droop-controlled interlinking converter is:

$$P_{IC} = \frac{1}{\vartheta_{IC}} (\hat{\omega} - \hat{V}_{dc}) \tag{3.38}$$

Where, "ϑ_{IC}" is droop gain for active power of interlinking converter and it determines the amount of active power transferred between AC and DC subgrids based on Δe. The direction of transferred power is specified based on the sign of Δe. If $\Delta e > 0$, power transferred from AC to DC subgrid, and if $\Delta e < 0$, power transferred from DC to AC subgrid. ϑ_{IC} can be determined as [37]:

$$\vartheta_{IC} = \frac{\hat{\omega}^{max} - \hat{\omega}^{min}}{P_{IC}^{max}} \tag{3.39}$$

Where, P_{IC}^{max} is the maximum capacity of the converter, and $\hat{\omega}^{max}$ and $\hat{\omega}^{min}$ are maximum and minimum normalized frequency or $+1$ and -1, respectively.

When there are multiple AC or DC subgrids, since the DC voltage and frequency might be different in each subgrid, each interlinking converter should have its own droop characteristics in order to control the direction and amount of power transferred between subgrids appropriately [37].

In an isolated AC/DC system, when the active power flows from the DC subgrid to the AC subgrid, the interlinking converter is also able to support the reactive power [70]. This reactive power can be controlled in a similar manner to droop-based AC DGs (equation (3.12)), if the converter limits are respected:

$$Q_{c_{lim}} = \sqrt{S_{c_{lim}}^2 - P_{IC}^2} \tag{3.40}$$

$$Q_c = \begin{cases} min\left(Q_{c_{lim}}, (V_c - V_{c_0})/\vartheta_{q_c}\right) & P_{IC} > 0 \\ 0 & P_{IC} \leq 0 \end{cases} \tag{3.41}$$

Where, "ϑ_{q_c}" is droop gain for reactive power of interlinking converter and it can be calculated in a similar manner as reactive power droop gain of AC DGs (equation (3.14)).

The droop control requires the continuous operation of the interlinking converter which would increase the conversion losses [38]. To overcome this shortcoming, the dead-zone (no power exchange zone) control strategy has been introduced [38]. In this control scheme the power exchange is only allowed when one of the subgrids is overloaded while the other is underloaded.

In addition to the mentioned modeling approaches for VSCs, another approach has been proposed for VSCs in load-flow studies based on the sequence components [40, 48]. As most of VSC controllers are implemented using sequence components, it might be more convenient to model the VSC in sequence frame [113]. The positive-sequence model of the VSC is employed for PQ or PV control modes, while the negative-sequence or zero-sequence model can provide some specific control functions such as injecting only balanced three phase current [113] or compensating the zero-sequence current of an unbalanced load [114].

In the mentioned modeling approaches for AC/DC converters in load-flow studies, these converters are usually modeled as voltage and current sources connected to AC and DC subgrids. However, there is also another modeling approach for such converters named as π-model. This model can be incorporated into the admittance matrix and results in modeling of the AC/DC system with multiple AC and DC sections and also a three-phase unbalanced AC/DC load-flow analysis using the Newton method [115].

3.1.2 Unified Modeling

Most of the research works on load-flow modeling of AC/DC power systems are based on the decoupled modeling concept [29-31, 33, 35, 37-39, 46, 47, 51, 54, 71, 107]. However, AC/DC power systems can be modeled as a unified system without decoupling of AC and DC parts [34]. This modeling approach might be more appropriate than the decoupled approach for AC/DC distribution systems as they consist of various types of AC and DC DGs and loads, and numerous AC and DC buses and lines merged with each other that cannot be decoupled easily [34].

Similar to decoupled modeling, in unified approach, VSCs are modeled based on the relations of their voltage [70] and power [107] at the AC and DC sides in both grid-connected and isolated cases.

As shown by equation (3.30), for a VSC with three-phase sinusoidal PWM in a linear modulation range ($M < 1$), if the positive and negative DC bus voltages are $+V_{dc}/2$ and $-V_{dc}/2$, the magnitude of AC bus voltage and its RMS value would be $MV_{dc}/2$ and $MV_{dc}/2\sqrt{2}$, respectively. Hence, the relation between base (i.e. $M = 1$) AC and DC voltages can be written as [109]:

$$V_{c,i}^{base} = \frac{1}{2\sqrt{2}} V_{dc,m}^{base} \tag{3.42}$$

Consequently, their relation in p.u. can be given by:

$$V_{c,i}^{pu} = M V_{dc,m}^{pu} \tag{3.43}$$

Moreover, VSC's DC and AC active power are related to each other by converter's efficiency (η):

$$P_c = \frac{P_{dc}}{\eta} = \frac{V_{dc,m} I_{dc,ml}}{\eta} \tag{3.44}$$

As shown by equation (3.15), the current $I_{dc,ml}$ which flows from DC bus "m" to DC bus "l" can be calculated as:

$$I_{dc,ml} = G_{dc,ml}(V_{dc,m} - V_{dc,l}) \tag{3.45}$$

Substituting (3.43) and (3.45) into (3.44) results in:

$$P_c = \frac{G_{dc}^{pu}}{\eta}(M^{-2}(V_{c,i}^{pu})^2 - M^{-1}V_{c,i}^{pu}V_{dc,l}^{pu}) \tag{3.46}$$

The reactive power at AC side of VSC (Q_c) can be controlled by a direct setpoint or calculated as:

$$Q_c = P_c \tan \varphi_c \tag{3.47}$$

where, φ_c is the power factor angle of the converter.

The other parts of the AC/DC distribution system are modeled according to the different AC/DC configurations. Four different cases are considered for the possible connection of AC and DC buses in an AC/DC distribution system and power equations are derived for each case [34]:

Case 1: connection between two AC buses via an AC line (Figure 3.7).

In this case, the active and reactive power equations between bus "i" and "j" are similar to conventional load-flow equations between two buses (i.e. (3.1) and (3.2)).

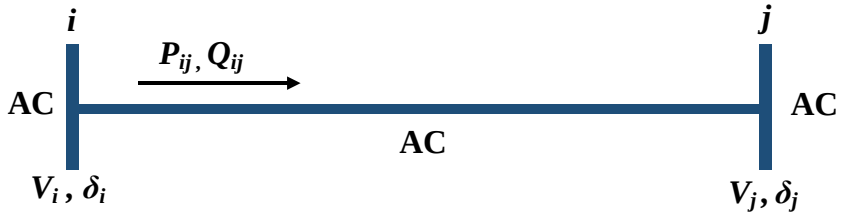

Figure 3.7 Connection between two AC buses via AC line [34]

Case 2: connection between two AC buses via a DC line and two AC/DC converters (Figure 3.8).

In this case, the active and reactive power equations between bus "i" and "j" are as follows:

$$P_{ij} = G_{dc,ij}(M_{ij}^{-2}V_i^2 - M_{ij}^{-1}\,V_i M_{ji}^{-1}\,V_j)(\frac{a_1}{\eta_{ij-r}} + b_1\eta_{ij-i}) \tag{3.48}$$

$$Q_{ij} = P_{ij}\,tan\,\varphi_{c-ij} \tag{3.49}$$

where, M_{ij} and φ_{c-ij} are the modulation index and power factor angle for the VSC connected to bus "i" between buses "i" and "j", respectively. Subscripts "r" and "i" in η_{ij} indicate if the VSC

functions as rectifier or inverter, respectively. Coefficients a_1 and b_1 can be determined using equations (3.52) and (3.53). When the VSC functions as a rectifier, $a_1 = 1$ and $b_1 = 0$, and when it functions as an inverter $a_1 = 0$ and $b_1 = 1$.

$$a_1 = 0.5(1 + \text{sgn}(M_{ij}^{-1} V_i - M_{ji}^{-1} V_j)) \tag{3.50}$$

$$b_1 = 0.5(1 - \text{sgn}(M_{ij}^{-1} V_i - M_{ji}^{-1} V_j)) \tag{3.51}$$

where, "sgn" is the sign function.

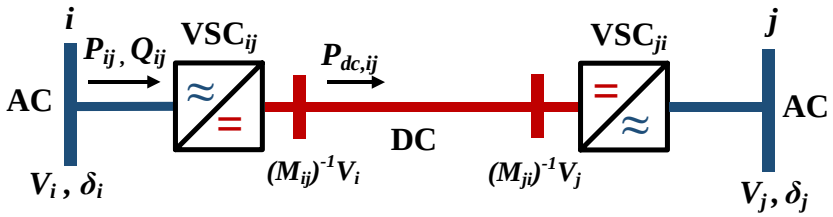

Figure 3.8 Connection between two AC buses via DC line and two AC/DC converters [34]

Case 3: connection between AC and DC buses (Figure 3.9 and Figure 3.10).

If the power flows from AC to DC, the active and reactive power equations between bus "*i*" and "*j*" are similar to previous case (i.e. equations (3.48) and (3.49)).

$$P_{ij} = G_{dc,ij}(M_{ij}^{-2} V_i^2 - M_{ij}^{-1} V_i V_j)(\frac{a_2}{\eta_{ij-r}} + b_2 \eta_{ij-i}) \tag{3.52}$$

$$Q_{ij} = P_{ij} \tan \varphi_{c-ij} \tag{3.53}$$

In these equations, all the parameters are similar to the previous case except a_2 and b_2 coefficients. They can be determined using equations (3.54) and (3.55). When the VSC functions as a rectifier, $a_2 = 1$ and $b_2 = 0$, and when it functions as an inverter $a_2 = 0$ and $b_2 = 1$.

$$a_2 = 0.5(1 + \text{sgn}(M_{ij}^{-1} V_i - V_j)) \tag{3.54}$$

$$b_2 = 0.5(1 - \text{sgn}(M_{ij}^{-1} V_i - V_j)) \tag{3.55}$$

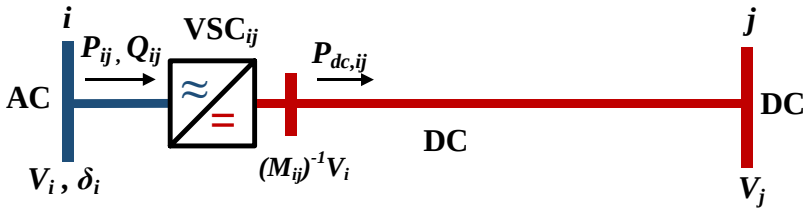

Figure 3.9 Connection between AC and DC buses (power flows from AC to DC) [34]

If the power flows from DC to AC, the power equation at DC bus "i" is as follows:

$$P_{ij} = G_{dc,ij}(V_i^2 - V_i M_{ji}^{-1} V_j) \tag{3.56}$$

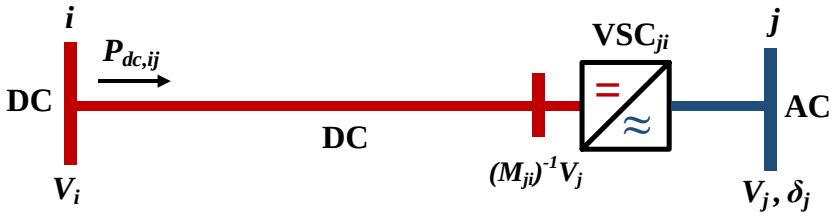

Figure 3.10 Connection between AC and DC buses (power flows from DC to AC) [34]

Case 4: connection between two DC buses (Figure 3.11).

In this case, the DC power equation between bus "i" and "j" is given by:

$$P_{ij} = G_{dc,ij}(V_i^2 - V_i V_j) \tag{3.57}$$

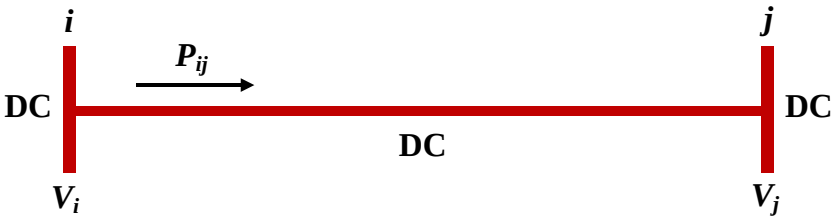

Figure 3.11 Connection between two DC buses [34]

3.2 AC/DC load-flow Problem Formulation and Solution Methods

The AC/DC load-flow problem is formulated based on the models derived for the AC/DC power system. This problem is formed as a set of mismatch equations which need to be solved iteratively until the difference between known and calculated values are lower than a specified value (pre-defined maximum mismatch). AC/DC load-flow equations might be set up in different formats based on the type of the AC/DC system (grid-connected or isolated) and the modeling approach (decoupled or unified). Furthermore, as stated in section 2.2, AC/DC load-flow equations can be solved using sequential or unified algorithms. These two methods of AC/DC load-flow solution are explained in more detail in the following.

In sequential AC/DC load-flow solution approach, the three sets of system equations (i.e. AC grid, DC grid, and interlinking converter) are solved separately. This method usually starts with estimation of DC system parameters. Afterwards, it finds the AC system equations solution and used it to modify the estimated DC parameters. After this modification, the whole AC system solution must be repeated. This iterative process continues until convergence is obtained [29]. The main advantage of the sequential method is that it requires lower computational requirements as it can be coded in existing load-flow analysis programs [42]. However, due to the additional iterative loops, the sequential method is more time consuming and it may have convergence problems in case one of the internal loops does not converge [43-45].

Several algorithms mostly based on the Newton iterative method have been proposed for the sequential load-flow analysis of AC/DC power systems [29, 32, 35, 39, 44, 46-49]. Figure 3.12 illustrates the flowchart of a sequential AC/DC load-flow algorithm. The steps required for the algorithm are as follows [47]:

1- DC slack converter is a converter station in the AC/DC system which it adopts its active power injection to control its DC bus voltage. Considering lossless DC grid and converter, an initial value is estimated for injecting power of DC slack converter. According to conservation of power, by neglecting losses, the estimated initial injecting power of the slack converter is equal to the sum of powers at the rest of converter buses.
2- Using the conventional Newton method in an inner loop, AC load-flow (based on equations (3.1) and (3.2)) is calculated until convergence is reached.

3- To accommodate converter stations into AC grid, AC load-flow equations must be extended by including converter active and reactive power injections into mismatch equations (this is similar to equations (3.58) and (3.59)). Hence, the active and reactive power injected to AC grid by converters along with converter losses are calculated based on the AC load-flow results (based on equations (3.32) and (3.33)). Consequently, the injected power to DC grid can be determined (using equation (3.34)).
4- DC load-flow is determined by solving the DC grid equation (i.e. equation (3.18)) in another inner loop using Newton method.
5- Based on the DC slack converter losses calculated in step 3 and its DC active power determined in step 4, the active power injected to AC grid by DC slack converter bus can be calculated based on equation (3.34).
6- The calculated active power injected to AC grid by DC slack converter in previous step is compared to its initial value which was estimated in step 1. If their difference is less than a pre-defined mismatch, the DC slack convergence criterion is fulfilled. Otherwise, with new calculated DC slack bus power, next iteration from step 2 is needed. Once the DC slack convergence criterion is fulfilled, the active and reactive power injections of DC slack bus can be calculated based on equations (3.1) and (3.2).

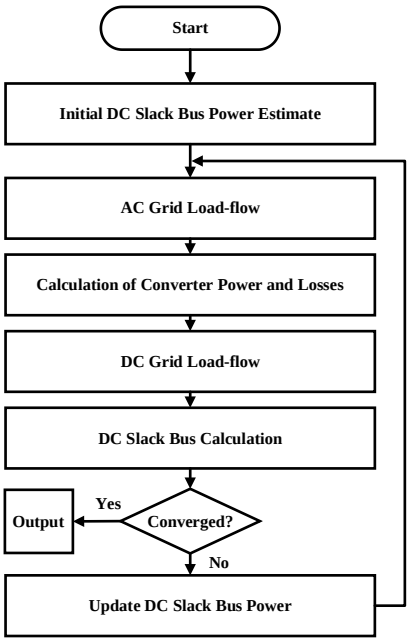

Figure 3.12 Flowchart of a sequential AC/DC load-flow algorithm

In unified load-flow method, all sets of AC/DC power system's equations are solved simultaneously. Several unified approaches have been proposed for load-flow analysis of AC/DC power systems [30, 33, 38, 51, 52, 54]. Similar to the sequential approach, the most commonly employed algorithms to solve the load-flow problems with unified approach are also based on Newton iterative method.

The flowchart of a unified AC/DC load-flow algorithm is shown in Figure 3.13. The steps required for the algorithm are as follows [43]:

1- Initialization of input variables. This includes a flat ($V_{ac}{}^{(0)} = 1.0\ p.u.$ and $\theta^{(0)} = 0.0°$) estimation of AC voltage magnitudes for load (PQ) buses, phase angle for all non-slack (PV and PQ) buses, and DC voltage magnitudes ($V_{dc}{}^{(0)} = 1\ p.u.$) for non-slack buses (DC load buses) in DC system. The initial value for total losses at DC slack converter bus is considered to be zero.
2- The initial AC active power of the slack converter is calculated. Since losses are neglected in previous step, this is equal to the DC power of the slack converter bus (similar to sequential method, DC slack converter has constant DC voltage) which can be determined based on equation (3.17).
3- Injected AC active and reactive power for each bus are calculated based on equations (3.1) and (3.2).
4- By finding out the injected current for each converter from the injected active and reactive power calculated in previous step, total loss for all converters can be determined using equations (3.32) and (3.33).
5- Injected and reference DC powers for non-slack converters (PV and PQ) are calculated based on equations (3.18) and (3.31) where AC active powers for non-slack converters are known and losses are calculated in step 4. The convergence of injected to reference DC power must be checked based on the DC mismatch equation which is the difference between these powers.
6- All the required data to obtain the three mismatch equations (AC, DC, and slack converter loss) are available. Hence, the convergence of this set of equations can be checked. If the convergence is not reached, all the input variables are updated for the next iteration.

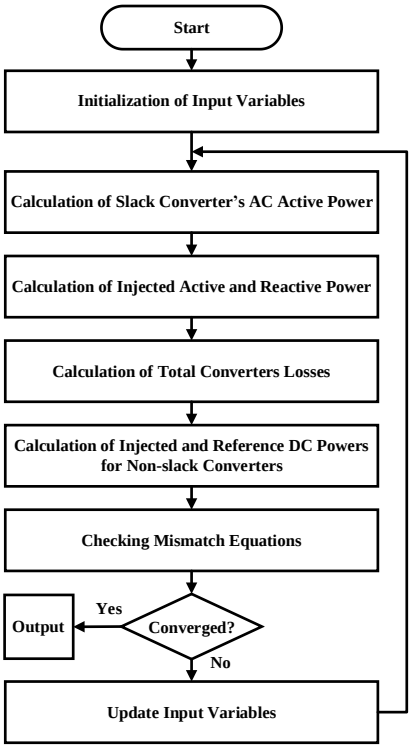

Figure 3.13 Flowchart of a unified AC/DC load-flow algorithm

In general, unified solution algorithm is superior to sequential algorithm due to its less computation time and more robust convergence features. Hence, this thesis mainly focused on unified solution for AC/DC load-flow problem.

In the following, two unified AC/DC load-flow problem formulation and solution procedures which are proposed for decoupled and unified modeling approaches are presented.

As mentioned in section 3.1.1, in decoupled modeling approach for load-flow analysis, the AC/DC distribution systems are divided into AC grid, DC grid, and the interlinking converter. In case the system under review is an isolated system from the utility grid, some additional equations such as droop equations for AC and DC DGs and interlinking converters must be added to grid-connected AC/DC load-flow equations. Therefore, by describing the load-flow formulation and solution method for an isolated AC/DC distribution system, grid-connected case is automatically explained.

One of the most straightforward unified algorithm for load-flow analysis of isolated AC/DC distribution system (islanded AC/DC microgrid) based on decoupled modeling approach proposed in [37]. Newton method is employed to solve this AC/DC load-flow problem. Based on the

equations mentioned in section 3.1.1 such as injected power to AC or DC buses and loads and DGs connected to each bus, power balance (mismatch) equations for any AC bus "i" and DC bus "m" can be formed as follows [37]:

$$P_{mis,i}^{ac} = P_{G,i}^{ac} + P_{IC,i}^{ac} - P_{L,i}^{ac} - P_{i}^{ac} \tag{3.58}$$

$$Q_{mis,i}^{ac} = Q_{G,i}^{ac} + Q_{IC,i}^{ac} - Q_{L,i}^{ac} - Q_{i}^{ac} \tag{3.59}$$

$$P_{mis,m}^{dc} = P_{G,m}^{dc} + P_{IC,m}^{dc} - P_{L,m}^{dc} - P_{m}^{dc} \tag{3.60}$$

Where, subscripts G, IC, and L represents generator, interlinking converter, and loads, respectively. P_i^{ac}, Q_i^{ac}, and P_m^{dc} are the injected powers at AC bus "i" and DC bus "m" and can be calculated based on equations (3.1), (3.2), and (3.18), respectively. These are generic mismatch equations and if some specific components are not connected to a bus, their corresponding terms in equations are equal to zero.

Considering a lossless operation for the interlinking converter due to the assumption that the AC/DC microgrid works at low or medium voltage levels, the power (mismatch) balance equation ($P_{mis,c}^{IC}$) at the AC side of the converter connected to bus "c" is [37]:

$$P_{mis,c}^{IC} = P_{G,c}^{ac} - P_{IC,c} - P_{L,c}^{ac} - P_{c}^{ac} \tag{3.61}$$

Here, it is assumed that $P_{IC} = P_{IC}^{\mathrm{dc}}$ where P_{IC}^{dc} is the active power injected by interlinking converter to DC grid. Therefore, based on equation (3.34), the active power injected by interlinking converter to AC grid is $P_{IC}^{\mathrm{ac}} = -P_{IC}^{\mathrm{dc}} = -P_{IC}$. Equation (3.61) indicates the interdependency of AC and DC grids. Since P_{IC} includes DC voltage terms, the AC power balance equation of the converter requires partial derivatives with respect to DC bus voltage.

Furthermore, the frequency is also an unknown variable in the load-flow analysis of the islanded AC/DC system. Hence, the partial derivatives of the power balance equations with respect to frequency must also be incorporated in the Jacobian matrix of the system. In this case, in order to equalize the number of mismatch equations and unknown variables, the voltage phase angle of one of the AC buses is considered as a reference and set to be zero.

Considering the aforementioned points, the Newton equations (Jacobian matrix and the updating equation) for this AC/DC load-flow method are as follows [37]:

$$\boldsymbol{J} = \begin{bmatrix} \frac{\partial \boldsymbol{P}_{\boldsymbol{mis}}^{\boldsymbol{ac}}}{\partial \boldsymbol{V}_{\boldsymbol{ac}}} & \frac{\partial \boldsymbol{P}_{\boldsymbol{mis}}^{\boldsymbol{ac}}}{\partial \boldsymbol{\omega}} & \frac{\partial \boldsymbol{P}_{\boldsymbol{mis}}^{\boldsymbol{ac}}}{\partial \boldsymbol{\delta}} & \frac{\partial \boldsymbol{P}_{\boldsymbol{mis}}^{\boldsymbol{ac}}}{\partial \boldsymbol{V}_{\boldsymbol{dc}}} \\ \frac{\partial \boldsymbol{Q}_{\boldsymbol{mis}}^{\boldsymbol{ac}}}{\partial \boldsymbol{V}_{\boldsymbol{ac}}} & \frac{\partial \boldsymbol{Q}_{\boldsymbol{mis}}^{\boldsymbol{ac}}}{\partial \boldsymbol{\omega}} & \frac{\partial \boldsymbol{Q}_{\boldsymbol{mis}}^{\boldsymbol{ac}}}{\partial \boldsymbol{\delta}} & \frac{\partial \boldsymbol{Q}_{\boldsymbol{mis}}^{\boldsymbol{ac}}}{\partial \boldsymbol{V}_{\boldsymbol{dc}}} \\ \frac{\partial \boldsymbol{P}_{\boldsymbol{mis}}^{\boldsymbol{dc}}}{\partial \boldsymbol{V}_{\boldsymbol{ac}}} & \frac{\partial \boldsymbol{P}_{\boldsymbol{mis}}^{\boldsymbol{dc}}}{\partial \boldsymbol{\omega}} & \frac{\partial \boldsymbol{P}_{\boldsymbol{mis}}^{\boldsymbol{dc}}}{\partial \boldsymbol{\delta}} & \frac{\partial \boldsymbol{P}_{\boldsymbol{mis}}^{\boldsymbol{dc}}}{\partial \boldsymbol{V}_{\boldsymbol{dc}}} \end{bmatrix} \tag{3.62}$$

$$\begin{bmatrix} \boldsymbol{V}_{\boldsymbol{ac}} \\ \boldsymbol{\omega} \\ \boldsymbol{\delta} \\ \boldsymbol{V}_{\boldsymbol{dc}} \end{bmatrix}^{k+1} = \begin{bmatrix} \boldsymbol{V}_{\boldsymbol{ac}} \\ \boldsymbol{\omega} \\ \boldsymbol{\delta} \\ \boldsymbol{V}_{\boldsymbol{dc}} \end{bmatrix}^{k} - \boldsymbol{J}^{-1} \begin{bmatrix} \boldsymbol{P}_{\boldsymbol{mis}}^{\boldsymbol{ac}} \\ \boldsymbol{Q}_{\boldsymbol{mis}}^{\boldsymbol{ac}} \\ \boldsymbol{P}_{\boldsymbol{mis}}^{\boldsymbol{dc}} \end{bmatrix}^{k} \tag{3.63}$$

where "k" is the iteration's number.

Similar to the conventional Newton AC load-flow, first, the Jacobian matrix of the system is formed (equation (3.62)), then the AC and DC voltage magnitudes, AC voltage phase angles and AC system frequency will be updated using equation (3.63). Consequently, power mismatch equations will be updated according to the updated unknown variables. This process will continue until the power mismatches are less than a specified value.

As stated in section 3.1.2, in contrast with decoupled approach, in unified approach the whole AC/DC network is modeled as a unified system [34]. Similar to the aforementioned load-flow solution, the AC/DC load-flow algorithm using unified modeling is also capable of being employed for isolated cases such as islanded AC/DC microgrids. In this method, in addition to AC admittance ($\boldsymbol{Y}$) and DC conductance ($\boldsymbol{G_{dc}}$) matrices, three binary configuration matrices ($\boldsymbol{W}, \boldsymbol{U}, \boldsymbol{D}$) are defined based on the configuration of an AC/DC power system with "N" buses [34]:

- $\boldsymbol{W(N \times 1)}$**:** Indicates the type of buses ($W_i = 0$ if bus "i" is AC, $W_i = 1$ if bus "i" is DC).
- $\boldsymbol{U(N \times N)}$**:** Illustrates the existence of connection between buses ($U_{ij} = 0$ if no line connects buses "i" and "j", $U_{ij} = 1$ if a line connects buses "i" and "j").
- $\boldsymbol{D(N \times N)}$**:** Describes the type of the lines between each two buses ($D_{ij} = 0$ if the line between buses "i" and "j" is AC, $D_{ij} = 1$ if the line between them is DC).

Moreover, the procedure of forming the AC admittance and DC conductance matrices is slightly different than the conventional method mentioned in section 3.1.1. For a system with N buses, Y_{ij} is an element in the $\boldsymbol{Y}$ matrix which represents the admittance of the AC line connecting buses "i" and "j". In contrast to the conventional procedure, the main diagonal of the $\boldsymbol{Y}$ matrix is equal to zero in this method. Furthermore, as the frequency is not constant in isolated cases, the admittance matrix must be considered as a function of frequency.

Similarly, for the same system with "N" buses, in the DC conductance matrix $\boldsymbol{G_{dc}}$, $G_{dc,ij}$ represents the conductance of the DC line between buses "i" and "j". Here, also the main diagonal of the $\boldsymbol{G_{dc}}$ matrix is equal to zero.

Once the input matrices are built, the active and reactive power balance (mismatch) equations can be written as follows [34]:

$$P_i^{inj} = P_i^{cal}, \qquad \forall i = 1,2,\dots,N \tag{3.64}$$

$$Q_i^{inj} = Q_i^{cal}, \qquad \forall i = 1,2,\dots,N \tag{3.65}$$

P_i^{inj} and Q_i^{inj} refer to the injected active and reactive power into bus "i" and they are calculated based on the generators and loads connected to that bus. P_i^{cal} and Q_i^{cal} refer to the active and reactive power transmitted through the lines connected to bus "i" which calculated based on the connection cases mentioned in section 3.1.2, and the configuration matrices ($\boldsymbol{W}$, $\boldsymbol{U}$, $\boldsymbol{D}$). The detailed formulas of injected and calculated powers are presented in Appendix B.

For the load-flow problem of isolated AC/DC systems, the power droop equations for AC and DC DGs as well as interlinking converters stated in section 3.1 are combined with injected and calculated active and reactive powers stated in (3.64) and (3.65). The reactive power droop equation of an interlinking converter connected to bus "i" can be obtained in a same manner as AC DGs (subscript "c" refers to the converter values) [34]:

$$Q_{c_{ac},i} = (V_{c_{ac_0},i} - V_{c_{ac},i})/\vartheta_{q_c,i} \tag{3.66}$$

The load-flow problem is formed by all the mismatch equations mentioned above as an optimization problem which required to be minimized and it can be solved simultaneously with

different methods such as Newton, or a Generalized Reduced Gradient (GRG) method [34]. The load-flow problem is formulated as [34]:

$$min\|F(x)\|_2 \qquad \text{x} \in R^{n_v} \tag{3.67}$$

Where, n_v is the number of system unknown variables x, and $F(x)$ is the set of mismatch equations and defined as [34]:

$$F(x) = \begin{cases} P_i^{inj} - P_i^{cal} & \forall i = 1,2,\dots,N \\ Q_i^{inj} - Q_i^{cal} & \forall i = 1,2,\dots,N \\ P_{G_{ac},i} - (\omega_0 - \omega)/\vartheta_{p_{ac},i} & \forall i = 1,2,\dots,N_{G_{ac}}^{dr} \\ Q_{G_{ac},i} - (V_{ac_0,i} - V_{ac,i})/\vartheta_{q_{ac},i} & \forall i = 1,2,\dots,N_{G_{ac}}^{dr} \\ P_{G_{dc},k} - (V_{dc_0,k} - V_{dc,k})/\vartheta_{P_{dc},k} & \forall i = 1,2,\dots,N_{G_{ac}}^{dr} \\ \hat{V}_{dc,i} - \hat{\omega} & \forall i = 1,2,\dots,N_c^{iso} \\ Q_{c_{ac},i} - (V_{c_{ac_0},i} - V_{c_{ac},i})/\vartheta_{q_c,i} & \forall i = 1,2,\dots,N_c^{iso} \end{cases} \tag{3.68}$$

The proposed algorithm to solve this load-flow problem is as follows [34]:

1. At first, the type, the known and the unknown parameters (i.e. voltage magnitude, phase angle, and active and reactive powers for AC buses and voltage magnitude and active power for DC buses) for each bus must be defined.
2. In the second step, the AC admittance, the DC conductance, and the configuration matrices are constructed.
3. Afterwards, the parameters are converted to per-unit values and a flat start is considered for unknown voltages ($V^{(0)} = 1.0\ p.u.$ and $\delta^{(0)} = 0.0°$).
4. These data are employed as the input of the load-flow problem formulated by power balance and VSC droop equations. Consequently, the load-flow problem is solved using an iterative method (e.g. Newton or GRG) until the following convergence criteria is met.

$$max\left(\begin{bmatrix} P_i^{inj} - P_i^{cal} \\ Q_i^{inj} - Q_i^{cal} \end{bmatrix}\right) < \varepsilon \tag{3.69}$$

Where, ε is the maximum pre-defined mismatch.

CHAPTER 4 LOAD-FLOW METHODS VALIDATION AND COMPARISON

In this chapter, firstly in section 4.1, the two AC/DC load-flow methods based on decoupled [37] and unified [34] modeling approaches which were presented in previous chapter are firstly programmed in MATLAB and then validated by comparing their results with a time-domain simulation tool (i.e. EMTP). In section 4.2, the performances of these load-flow methods are compared to each other based on their results obtained from a specific case study. Consequently, in section 4.3 two techniques are introduced and applied to the aforementioned AC/DC load-flow methods in order to improve their performances.

In the following sections, for ease of reference, selected load-flow methods based on decoupled and unified modeling approaches will be referred as “decoupled” and “generalized” load-flow methods, respectively.

4.1 Validation of AC/DC Load-Flow Methods

In this section, the results of decoupled and generalized AC/DC load-flow methods are first being reproduced in MATLAB and then verified against the EMTP load-flow tool and steady-state solution of EMTP.

4.1.1 Validation of Decoupled AC/DC Load-Flow Method

In order to validate the mentioned decoupled AC/DC load-flow method, which is developed only for islanded AC/DC systems, one of the AC/DC test systems in the research work [37] is chosen. The 12-bus AC/DC system ($Test\_1$) is shown in Figure 4.1 and its parameters (impedances, loads, DGs, and converter) are stated in Table 4.1, Table 4.2, and Table 4.3. In this test system, AC lines are modeled as RL (resistance and inductance) branches and DC lines as R (resistance) branches. Although the reason is not stated in [37], but this might be due to considering short lines in load-flow analysis for low- or medium-voltage systems. In a similar case study in another research work on load-flow analysis of AC/DC microgrids, the lengths of lines are considered to be in the range of $0.05\,km$ to $0.1\,km$ [38]. These values illustrate that lines are assumed to be short in such systems, and they can be modeled as RL and R branches for AC and DC types, respectively.

The base values (apparent power, AC and DC voltages) for p.u. conversion are $S_{base} = 1\ kVA$, $V_{base}^{ac} = 127\ V$, and $V_{base}^{dc} = 400\ V$. Moreover, the acceptable voltage and frequency range for the system are $\pm 5\%$ and $\pm 2\%$, respectively. Although the AC base voltage is not a common value for low-voltage AC systems, but the main purpose here is to validate the decoupled load-flow method based on its results. Hence, all the above-mentioned base values are considered here.

This system comprises two 6-bus AC and DC subgrids which are connected to each other via an interlinking converter. Each subgrid consists of droop-controlled DGs and loads and the droop gains which are stated in Table 4.3, can be calculated as stated in previous chapter. It is also worth mentioning that the injected active and reactive powers of DGs and interlinking converter are assumed to be zero in decoupled load-flow method [37]. Hence, those powers can be determined using droop equations stated in section 3.1.1 at the end of the algorithm.

Table 4.1 Impedances of $Test\_1$ system

From Bus	To Bus	Resistance (Ω)	Inductance (mH)
1	2	0.02	0.12732
2	3	0.06	0.38197
3	6	0.01	0.06366
4	1	0.08	0.50930
5	2	0.04	0.25465
7	8	0.1	-
8	9	0.2	-
7	10	0.05	-
9	12	0.05	-
10	11	0.02	-
11	12	0.2	-

Table 4.2 Load data of $Test\_1$ system

Bus	$P_L^{ac}(kW)$	$Q_L^{ac}(kVAr)$	$P_L^{dc}(kW)$
1	1.614	1.068	-
3	2.145	1.516	-
7	-	-	10
11	-	-	7.3
12	-	-	7.3

Table 4.3 DGs and converter parameters of $Test\_1$ system

AC DGs	$S_{DG} = 1.6\ kVA, V_{DG} = 127\ V, 1\Phi, 50\ Hz$ $1/\vartheta_{p_{ac}} = 10638\ W/rads^{-1}, 1/\vartheta_{q_{ac}} = 1087.9\ VAr/V$
DC DGs	$15\ kW, 400\ V$ $1/\vartheta_{P_{dc}} = 10000\ W/V$
Converter (IC)	$\mathrm{P}_{IC,max} = 1.33\ kW$ $\vartheta_{IC} = 0.0015\ W^{-1}, \vartheta_{qIC} = 9.1924 \times 10^{-4}\ V/VAr$

The first step of the validation is done by reproducing the load-flow results of the above-mentioned AC/DC microgrid (obtained results in [37]) which is accomplished by programing the algorithm in MATLAB ($Codes\ Package\backslash Decoupled\ LF\backslash 12\ Bus\ Islanded\ Test\ System\backslash Test\_1.m$) using Newton method. With pre-defined maximum mismatch of 10^{-6}, the load-flow algorithm has reached convergence after 201 iterations and with mismatch of 9.8272×10^{-7}. Detailed load-flow results are stated in Table 4.4. As noted, the number of iterations is quite high compared to Newton load-flow solution for a conventional AC system which is usually converged within less than 10 iterations [116]. This could have several reasons such as variable frequency and its impact on AC voltages and admittances, or the load-flow modeling approach. The other possible reason which is frequently stated in the literature is that the Newton load-flow method works more efficiently and converges faster for power systems with higher X/R ratio such as high-voltage transmission systems. Since this ratio is lower in distribution system (with medium- or low-voltage level), Newton method requires a greater number of iterations for convergence [117].

As stated in previous chapter, in order to equalize the number of mismatch equations and unknown variables in isolated cases (where frequency is an unknown variable), one of the AC buses (e.g. bus 1) is considered as a reference with known phase angle ($\delta_1 = 0°$).

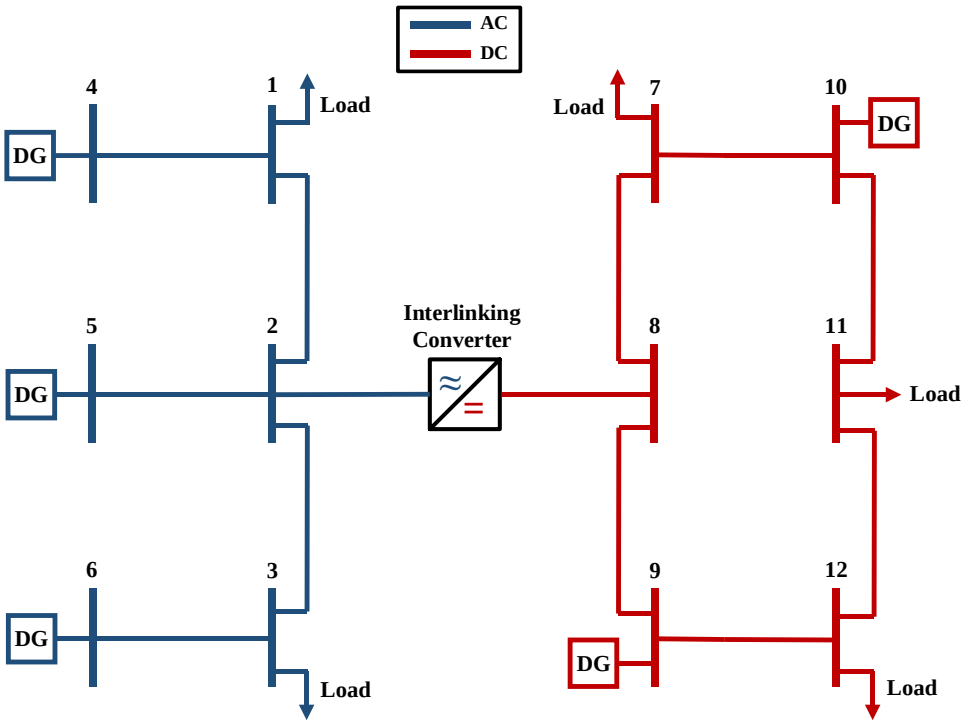

Figure 4.1 12-bus islanded AC/DC system ($Test\_1$) [37]

Table 4.4 Decoupled load-flow results of $Test\_1$ system

Bus	**Bus Type**	$\boldsymbol{V}$ $(\boldsymbol{p.u.})$	$\boldsymbol{\delta}$ (°)	$\boldsymbol{P_{ac}}$ $(\boldsymbol{p.u.})$	$\boldsymbol{Q_{ac}}$ $(\boldsymbol{p.u.})$	$\boldsymbol{P_{dc}}$ $(\boldsymbol{p.u.})$
1	AC Load	0.9908	0	-1.6140	-1.0680	-
2	IC (AC)	0.9935	-0.0160	-0.0532	0.8991	-
3	AC Load	0.9884	-0.3408	-2.1450	-1.5160	-
4	AC DG	0.9988	0.6841	1.2770	0.1720	-
5	AC DG	0.9980	0.3107	1.2770	0.2744	-
6	AC DG	0.9908	-0.2945	1.2770	1.2763	-
7	DC Load	0.9937	-	-	-	-10.0000
8	IC (DC)	0.9951	-	-	-	0.0532
9	DC DG	0.9976	-	-	-	9.4219
10	DC DG	0.9962	-	-	-	15.1764
11	DC Load	0.9953	-	-	-	-7.3000
12	DC Load	0.9953	-	-	-	-7.3000
f = 49.9809 Hz				No. of iterations = 201		
Mismatch = 9.8272×10^{-7} , Maximum mismatch = 10^{-6}						

The second step of the validation is done using EMTP. This start with performing an approximation using EMTP load-flow tool for the AC subgrid. The AC DGs are considered as PV buses in EMTP with typical active power and voltage magnitude values $P = 0.8\, S_{DG}$ (typical DG sets rated power factor is $\cos\emptyset = 0.8$) and $V = 1\, p.u.$ respectively. Moreover, the interlinking converter is considered as slack bus with typical voltage magnitude and phase angle of $V = 1.0\, p.u.$ and $\delta = 0.0°$. Loads (PQ buses in EMTP) have same values as shown in Table 4.2. These approximations are considered to observe the impact of droop equations for AC DGs and interlinking converter on load-flow results. The EMTP load-flow results of AC subgrid based on the above-mentioned approximations are shown in Table 4.5. By comparing the results state in Table 4.4 and Table 4.5 it is noticed that the calculated voltage magnitudes, phase angles, and active powers using the approximations are slightly different than those determined by the MATLAB code. This illustrates that droop equations do not significantly impact the load-flow results. Therefore, it is reasonable to assume droop-based AC DGs as PV constraints in a conventional AC load-flow. However, calculated reactive powers by these two approaches are much more different. This can be explained by high sensitivity of reactive power to changes in voltage magnitudes. It is also the idea behind the fast decoupled AC load-flow method in which the couplings between $V\&P$ and $Q\&\delta$ are neglected [118].

Table 4.5 EMTP load-flow results for AC subgrid of $Test\_1$ system with PV approximation

Bus	**Bus Type**	$\boldsymbol{V}$ $(\boldsymbol{p.u.})$	$\boldsymbol{\delta}$ (°)	$\boldsymbol{P_{ac}}$ $(\boldsymbol{p.u.})$	$\boldsymbol{Q_{ac}}$ $(\boldsymbol{p.u.})$
1	AC Load (PQ)	0.9962	0.0456	-1.6140	-1.0680
2	IC (Slack)	1.0000	0	-0.0597	1.9243
3	AC Load (PQ)	0.9972	-0.3851	-2.1450	-1.5160
4	AC DG (PV)	1.0000	0.8486	1.28	-0.2518
5	AC DG (PV)	1.0000	0.4538	1.28	-0.6337
6	AC DG (PV)	1.0000	-0.3505	1.28	1.5877

In order to further verify the accuracy of the load-flow results for AC subgrid of $Test\_1$ system obtained in MATLAB (Table 4.4), the following steps are done in EMTP load-flow tool (Figure 4.2). The interlinking converter AC side (bus 2) is considered as slack bus with known voltage magnitude and phase angle from load-flow results. AC loads (buses 1 and 3) are PQ buses in EMTP, and AC DGs (buses 4, 5, and 6) are considered as PV buses with active power and voltage

magnitude obtained from MATLAB load-flow results. By running EMTP's load-flow, other unknown values of buses are obtained. For DC subgrid, DGs and DC side of interlinking converter are considered as DC voltage sources, and loads are represented by their equivalent resistances. The voltage magnitudes of these DC sources and the resistance values of the loads can be determined using the load-flow results obtained in MATLAB (Table 4.4). Therefore, the remaining unknown values for each bus are obtained by running time-domain simulation of the system in EMTP and reading the steady-state results. Table 4.6 shows the EMTP results for $Test\_1$ system. By comparing the results of the coded load-flow (Table 4.4) and EMTP (Table 4.6) the accuracy of the decoupled AC/DC load-flow algorithm can be verified.

Table 4.6 EMTP results for $Test\_1$ system

Bus	**Bus Type**	$\boldsymbol{V}$ $(\boldsymbol{p.u.})$	$\boldsymbol{\delta}$ (°)	$\boldsymbol{P_{ac}}$ $(\boldsymbol{p.u.})$	$\boldsymbol{Q_{ac}}$ $(\boldsymbol{p.u.})$	$\boldsymbol{P_{dc}}$ $(\boldsymbol{p.u.})$
1	AC Load	0.9908	0	-1.6140	-1.0680	-
2	IC (AC)	0.9935	-0.0160	-0.0532	0.8991	-
3	AC Load	0.9884	-0.3408	-2.1450	-1.5160	-
4	AC DG	0.9988	0.6841	1.2770	0.1720	-
5	AC DG	0.9980	0.3107	1.2770	0.2744	-
6	AC DG	0.9908	-0.2945	1.2770	1.2763	-
7	DC Load	0.9937	-	-	-	-10.0000
8	IC (DC)	0.9951	-	-	-	0.0532
9	DC DG	0.9976	-	-	-	9.4219
10	DC DG	0.9962	-	-	-	15.1764
11	DC Load	0.9953	-	-	-	-7.3000
12	DC Load	0.9953	-	-	-	-7.3000

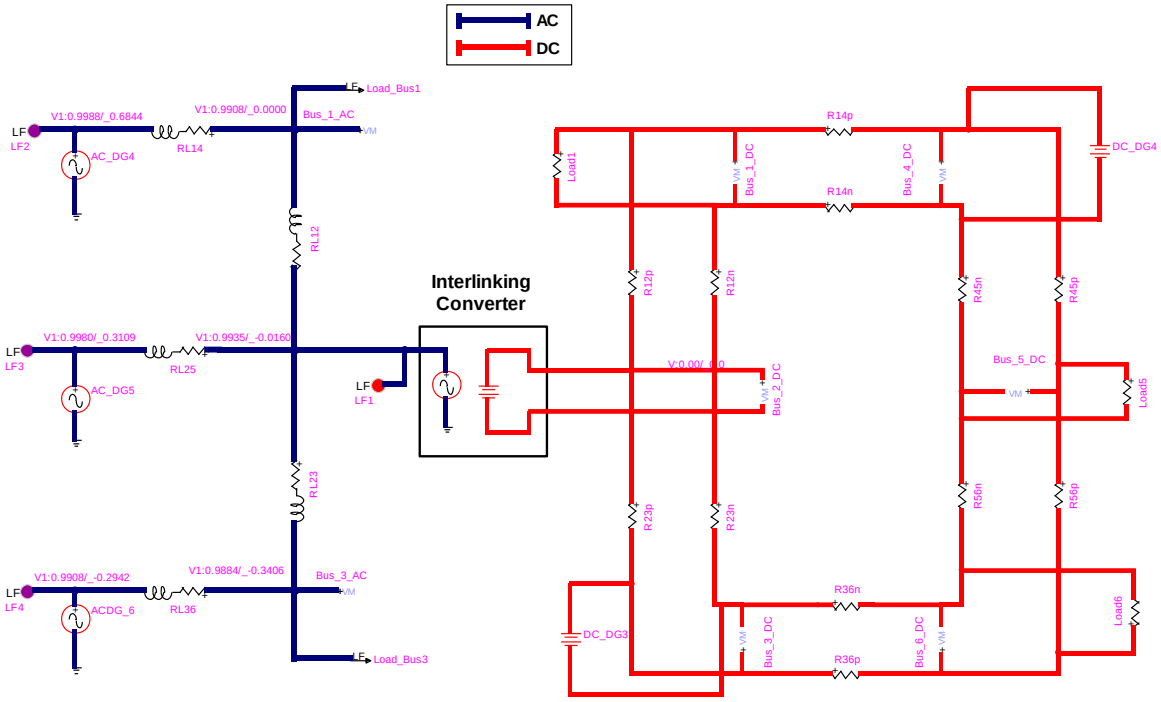

Figure 4.2 12-bus islanded AC/DC system ($Test\_1$) EMTP load-flow tool

4.1.2 Validation of Generalized AC/DC Load-Flow Method

In contrast with the above-mentioned decoupled AC/DC load-flow, the generalized AC/DC load-flow is developed for both grid-connected and islanded AC/DC systems. Hence, this load-flow method is validated based on two different case studies (grid-connected and islanded). The validation procedure is similar to what presented in the previous section.

4.1.2.1 Validation of Generalized Grid-Connected AC/DC Load-Flow

First, the generalized load-flow algorithm for a grid-connected AC/DC system (case study done in [34]) is programmed in MATLAB ($Codes\ Package\backslash Generalized\ LF\backslash 13-Bus\ Grid-Connected\backslash Test\_2.m$) and its results are reproduced. Afterwards, to verify the accuracy of the proposed method, the load-flow results are compared with the EMTP load-flow tool for AC parts and steady-state results obtained by simulating the AC/DC system ($Test\_2$) in EMTP for DC parts.

$Test\_2$ is a 13-bus AC/DC system shown in Figure 4.3 and its impedances which are modeled as RL and R branches for AC and DC lines are presented in Table 4.7. The base values (apparent

power, AC and DC voltages) for p.u. conversion are $S_{base} = 10\,MVA$, $V_{base}^{ac} = 4.16\,kV$, and $V_{base}^{dc} = 6.8\,kV$. The efficiency and power factor of VSCs are $\eta_c = 98\%$ and $\cos\varphi_c = 0.95$ and their modulation indices (M) are shown in Figure 4.3. Although the lines' length is not mentioned for this test system, but based on 13-bus IEEE test system with similar voltage level ($4.16\,kV$), lines length could be assumed to be between $90\,m$ to $600\,m$ [119]. In the load-flow algorithm, it is assumed that the injected active and reactive power of VSC buses are equal to zero [34]. However, VSCs' powers can be calculated based on the obtained load-flow results and using equations (3.46) and (3.47).

In this system, bus 1 is AC slack bus, bus 5 is DC voltage bus, bus 3 and bus 8 are AC PV buses, buses 10-13 are VSC buses, and the rest are AC or DC load buses. PV and load buses data are presented in

Table 4.8 and Table 4.9, respectively.

Table 4.7 Impedances of grid-connected $Test\_2$ system

From Bus	To Bus	Resistance (Ω)	Inductance (Ω)
1	2	0.2218	0.3630
1	9	0.2218	0.3630
2	3	0.8870	1.4520
3	10	0.0500	0.7540
3	11	0.0500	0.7540
4	5	0.2208	-
4	11	0.4415	-
5	6	0.2208	-
6	13	0.4415	-
7	8	0.4435	0.7260
7	12	0.0500	0.7540
7	13	0.0500	0.7540
8	9	0.4435	0.7260
10	12	0.8830	-

Table 4.8 PV buses data of grid-connected $Test\_2$ system

Bus	$V\ (p.u.)$	$P_G^{ac}(MW)$	$Q_{L,min}^{ac}(MVAr)$	$Q_{L,max}^{ac}(MVAr)$	$P_L^{ac}(MW)$	$Q_L^{ac}(MVAr)$
3	1.0	2.5	0.1	0.75	1.5	0.2
8	1.0	2.5	0.1	0.75	1.0	0.1

Table 4.9 Load buses data of grid-connected $Test\_2$ system

Bus	$P_L^{ac}(MW)$	$Q_L^{ac}(MVAr)$	$P_L^{dc}(MW)$
2	2.0	0.4	-
4	-	-	1.0
6	-	-	1.0
7	2.5	0.5	-
9	2.5	0.5	-

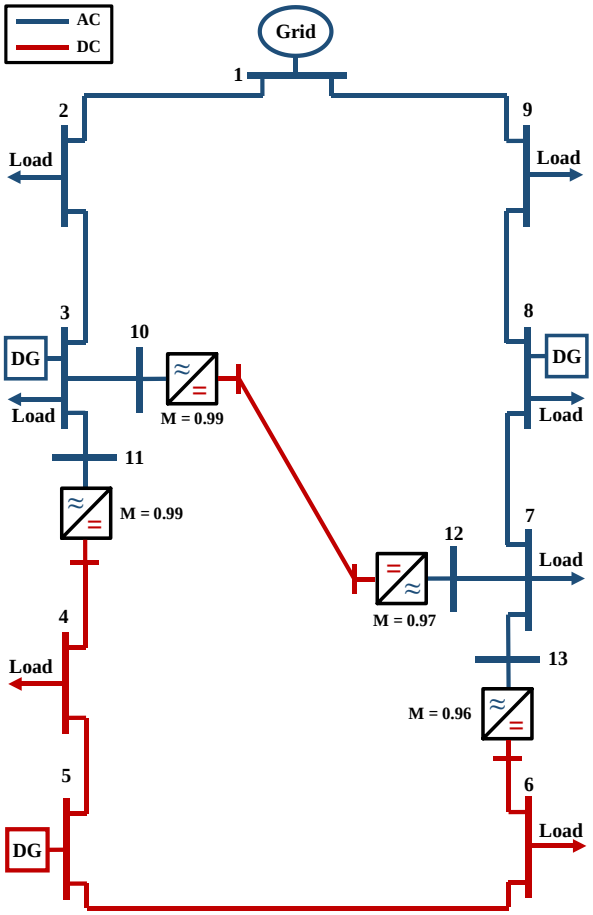

Figure 4.3 13-bus grid-connected AC/DC system ($Test\_2$) [34]

By programing the generalized AC/DC load-flow algorithm for the $Test\_2$ system using Newton method in MATLAB ($Codes\ Package\backslash Generalized\ LF\backslash 13-Bus\ Grid-Connected\backslash Test\_2.m$), it is noted that with the pre-defined maximum mismatch of 10^{-6}, the algorithm has reached convergence after 6 iterations (that is within a normal range as conventional AC load-flow solutions) and with mismatch of 4.7192×10^{-7}. The load-flow results are stated in Table 4.10.

The next step of validation is done using EMTP load-flow tool for AC parts of the system and EMTP steady-state results for its DC parts. Since $Test\_2$ system is a grid-connected system, its load-flow procedure in EMTP is straightforward. Similar to $Test\_1$, we can consider the AC side of interlinking converter (or VSC) buses as slack (or their equivalent PQ constraints calculated based on equations (3.46) and (3.47)) with voltage magnitude and phase angles known from the load-flow code programmed in MATLAB. The other AC buses (grid slack, PV, and PQ buses) are considered as they are in EMTP (Figure 4.4). By running the load-flow in EMTP, the unknown values for all the AC buses are calculated (Table 4.11).

For DC parts, DC loads are represented by resistances and DC DGs and DC sides of VSCs by DC voltage sources. After running time-domain simulation of the system, the unknown values for DC parts are determined based on the steady-state results (Table 4.11). By comparing load-flow results obtained in MATLAB (Table 4.10) and results achieved by EMTP load-flow tool and steady-state solution (Table 4.11), the accuracy of the generalized load-flow method for the grid-connected AC/DC test system ($Test\_2$) is verified.

Table 4.10 Generalized load-flow results of $Test\_2$ system

Bus	**Bus Type**	$\boldsymbol{V}$ $(\boldsymbol{p.u.})$	$\boldsymbol{\delta}$ (°)	$\boldsymbol{P_{ac}}$ $(\boldsymbol{p.u.})$	$\boldsymbol{Q_{ac}}$ $(\boldsymbol{p.u.})$	$\boldsymbol{P_{dc}}$ $(\boldsymbol{p.u.})$
1	AC, Slack	1.0500	0.0000	0.4921	0.1240	-
2	AC, Load	1.0126	-2.0717	-0.2000	-0.0400	-
3	AC, P-V	1.0000	-2.4360	0.1000	0.0325	-
4	DC, Load	0.9974	-	-	-	-0.1000
5	DC, Voltage	1.0000	-	-	-	0.1870
6	DC, Load	0.9937	-	-	-	-0.1000
7	AC, Load	0.9456	-6.6433	-0.2500	-0.0500	-
8	AC, P-V	1.0000	-2.9841	0.1500	0.0324	-
9	AC, Load	1.0043	-2.6574	-0.2500	-0.0500	-
10	AC, VSC	0.9882	-4.0539	-0.0655	-0.0215	-
11	AC, VSC	0.9917	-3.5826	-0.0466	-0.0153	-
12	AC, VSC	0.9563	-4.9660	0.0621	0.0204	-
13	AC, VSC	0.9510	-5.8077	0.0308	0.0101	-
f = 60 Hz				No. of iterations = 6		
Mismatch = 4.7192×10^{-7} , Maximum mismatch = 10^{-6}						

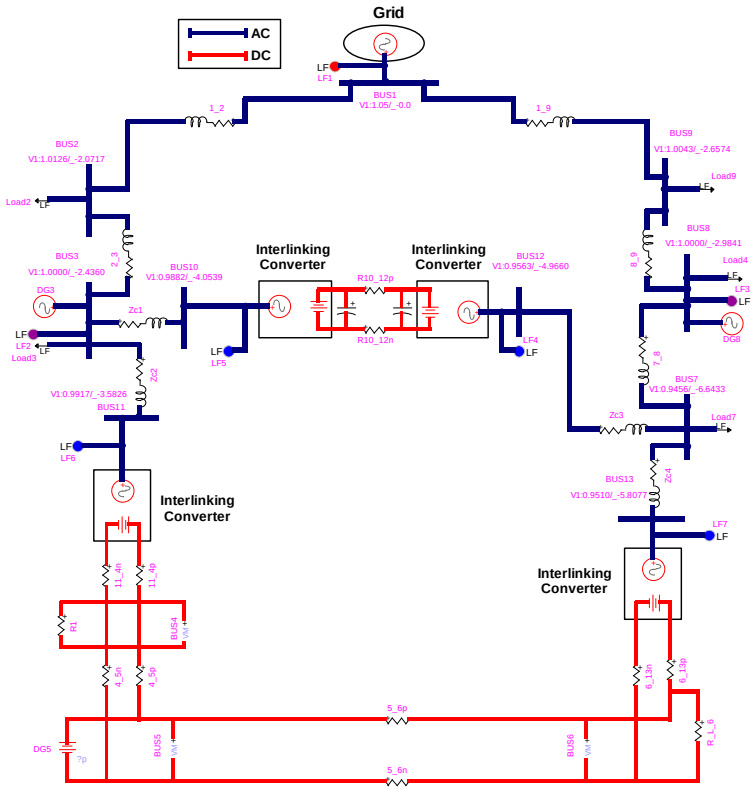

Figure 4.4 13-bus grid-connected AC/DC system ($Test\_2$) schematic in EMTP

Table 4.11 EMTP results of $Test\_2$ system

Bus	**Bus Type**	$\boldsymbol{V}$ $(\boldsymbol{p.u.})$	$\boldsymbol{\delta}$ (°)	$\boldsymbol{P_{ac}}$ $(\boldsymbol{p.u.})$	$\boldsymbol{Q_{ac}}$ $(\boldsymbol{p.u.})$	$\boldsymbol{P_{dc}}$ $(\boldsymbol{p.u.})$
1	AC, Slack	1.0500	0.0000	0.4921	0.1240	-
2	AC, Load	1.0126	-2.0717	-0.2000	-0.0400	-
3	AC, P-V	1.0000	-2.4360	0.1000	0.0325	-
4	DC, Load	0.9975	-	-	-	-0.1000
5	DC, Voltage	1.0000	-	-	-	0.1853
6	DC, Load	0.9936	-	-	-	-0.1000
7	AC, Load	0.9456	-6.6433	-0.2500	-0.0500	-
8	AC, P-V	1.0000	-2.9841	0.1500	0.0327	-
9	AC, Load	1.0043	-2.6574	-0.2500	-0.0500	-
10	AC, VSC	0.9882	-4.0539	-0.0655	-0.0215	-
11	AC, VSC	0.9917	-3.5826	-0.0466	-0.0153	-
12	AC, VSC	0.9563	-4.9660	0.0621	0.0204	-
13	AC, VSC	0.9510	-5.8077	0.0308	0.0101	-

4.1.2.2 Validation of Generalized Islanded AC/DC Load-Flow

Similar to the grid-connected case study, in order to validate the accuracy of the generalized load-flow method for islanded AC/DC systems, the results of a test system (case study done in [34]) must be verified against the EMTP load-flow tool for AC parts and steady-state solution for DC parts of the system. The 10-bus islanded AC/DC system ($Test\_3$) is shown in Figure 4.5 and its parameters (impedances, DGs and converters, and loads) are presented in Table 4.12, Table 4.13, and Table 4.14.

$Test\_3$ system is selected from a modified version of IEEE 33-bus test system (which firstly proposed in [120]) and the AC lines' impedances are chosen from IEEE 33-bus system [34]. The lines' length is not stated in neither [34] and [120]. However, they are considered to be short lines and like the previous cases, AC lines and DC lines are modeled as RL and R branches, respectively.

The base values (apparent power, AC and DC voltages) for p.u. conversion are $S_{base} = 10\ MVA$, $V_{base}^{ac} = 12.66\ kV$, and $V_{base}^{dc} = 20.67\ kV$. The efficiency and power factor of converters are $\eta_c = 95\%$ and $\cos\varphi_c = 0.95$ and modulation indices (M) of converters are presented in Figure 4.5. Moreover, acceptable voltage and frequency range for the system are $\pm 5\%$ and $\pm 1\%$, respectively. Similar to $Test\_1$ system, here also the injected active and reactive power for DGs and converters are assumed to be zero, and these power can be determined using droop equations at the end of the generalized load-flow algorithm for islanded AC/DC systems [34].

Table 4.12 Impedances of $Test\_3$ system

From Bus	To Bus	Resistance (Ω)	Inductance (Ω)
1	2	0.5910	0.5260
2	3	1.4926	-
2	8	2.0000	2.0000
3	4	2.5780	-
4	5	1.4640	-
5	10	1.0000	-
6	7	0.5075	0.2585
7	8	0.9744	0.9630
8	9	0.3105	0.3619
9	10	0.3410	0.5302

Table 4.13 DGs and converter parameters of $Test\_3$ system

AC DGs	Bus 6	$\vartheta_{p_{ac}} = 0.4\ p.u.,\ \vartheta_{q_{ac}} = 4\ p.u.$
	Bus 8	$\vartheta_{p_{ac}} = 0.16\ p.u.,\ \vartheta_{q_{ac}} = 2\ p.u.$
DC DGs	Bus 3	$\vartheta_{p_{dc}} = 1.333\ p.u.$
	Bus 4	$\vartheta_{p_{dc}} = 4\ p.u.$
Converter	Bus 2	$\vartheta_{IC} = 4\ p.u.,\ \vartheta_{qIC} = 2.5\ p.u.$
	Bus 10	$\vartheta_{IC} = 4\ p.u.,\ \vartheta_{qIC} = 2.5\ p.u.$

Table 4.14 Load data of $Test\_3$ system

Bus	$\boldsymbol{P_L^{ac}(kW)}$	$\boldsymbol{Q_L^{ac}(kW)}$	$\boldsymbol{P_L^{dc}(kW)}$
1	400	200	-
2	260	105	-
3	-	-	60
4	-	-	60
5	45	20	45
6	85	35	-
7	100	60	100
8	170	50	-
9	145	70	145
10	240	160	-

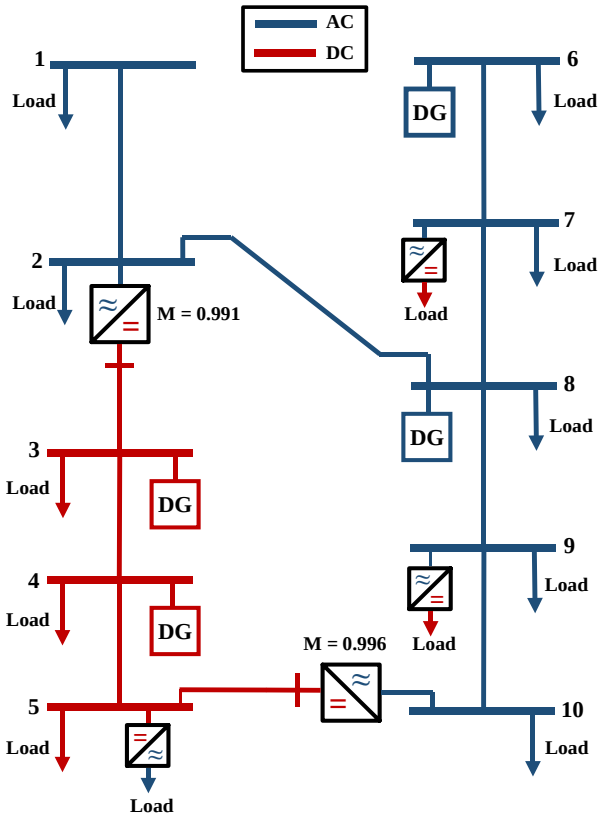

Figure 4.5 10-bus islanded AC/DC system ($Test\_3$) [34]

The generalized AC/DC load-flow algorithm for the islanded 10-bus test system with aforementioned parameters is programmed in MATLAB ($Codes\ Package\backslash Generalized\ LF\backslash 10-Bus\ Islanded\backslash Test\_3.m$) using Newton method. As shown in Table 4.15,it is noted that with the pre-defined maximum mismatch of 10^{-6}, the algorithm has reached convergence after 53 iterations and with mismatch of 9.4102×10^{-7}. Compared to previous grid-connected case ($Test\_2$), generalized load-flow solution for the $Test\_3$ system needs to iterate more until it converges. This could be due to the variation in the system's frequency and its impact on admittances and voltages.

Similar to the decoupled AC/DC load-flow method, in order to equalize the number of mismatch equations and unknown variables in an isolated system (where the frequency is an unknown load-flow variable), one of the AC buses (e.g. bus 8) is considered as a reference with known phase angle ($\delta_8 = 0°$).

Table 4.15 Generalized load-flow results of $Test\_3$ system

Bus	**Bus Type**	$\boldsymbol{V}$ $(\boldsymbol{p.u.})$	$\boldsymbol{\delta}$ (°)	$\boldsymbol{P_{ac}}$ $(\boldsymbol{p.u.})$	$\boldsymbol{Q_{ac}}$ $(\boldsymbol{p.u.})$	$\boldsymbol{P_{dc}}$ $(\boldsymbol{p.u.})$
1	AC Load	0.9539	-0.0884	-0.0400	-0.0200	-
2	IC (AC)	0.9561	-0.0523	0.0152	0.0071	-
3	DC DG	0.9651	-	-	-	0.0202
4	DC DG	0.9643	-	-	-	0.0029
5	DC Load	0.9638	-	-	-	-0.0092
6	AC DG	0.9598	-0.0290	0.0132	0.0065	-
7	AC Load	0.9593	-0.0293	-0.0205	-0.0060	-
8	AC DG	0.9597	0	0.0373	0.0151	-
9	AC Load	0.9593	-0.0117	-0.0298	-0.0070	-
10	IC (AC)	0.9598	0.0208	0.0115	0.0001	-
f = 59.4785 Hz				No. of iterations = 53		
Mismatch = 9.4102×10^{-7} , Maximum mismatch = 10^{-6}						

The validation procedure for the generalized load-flow method for islanded AC/DC systems is similar to previous islanded test case ($Test\_1$). For the AC parts of the system, EMTP load-flow tool is employed in a similar manner for $Test\_1$ system in which AC DGs are considered as PV buses and AC sides of converters as slack buses with values obtained from the load-flow algorithm programmed in MATLAB. Similar to $Test\_1$ system, for DC parts, the steady-state results obtained in EMTP can be compared with corresponding values calculated in the load-flow code. The schematic of the $Test\_3$ system in EMTP is shown in Figure 4.6. Table 4.16 presents the EMTP results which includes both AC load-flow and DC steady-state solutions of $Test\_3$. By comparing the active and reactive powers of VSCs (buses 2 and 10) in Table 4.15 and Table 4.16, it is noticed that they have different values in EMTP and MATLAB. The reason is that in generalized method, the whole AC/DC system is modeled with unified approach and the contribution of DC subgrid is considered in load-flow algorithm coded in MATLAB. However, in EMTP it is assumed that the system is divided to two separate AC and DC systems and the slack buses (VSCs) in EMTP must compensate the DC subgrid contribution and balance the active and reactive powers in AC subgrid.

By comparing the results for all of the other buses in Table 4.15 and Table 4.16, the accuracy of the generalized load-flow method for islanded AC/DC systems can be verified.

Table 4.16 EMTP results of $Test\_3$ system

Bus	**Bus Type**	$\boldsymbol{V}$ $(\boldsymbol{p.u.})$	$\boldsymbol{\delta}$ (°)	$\boldsymbol{P_{ac}}$ $(\boldsymbol{p.u.})$	$\boldsymbol{Q_{ac}}$ $(\boldsymbol{p.u.})$	$\boldsymbol{P_{dc}}$ $(\boldsymbol{p.u.})$
1	AC Load	0.9539	-0.0892	-0.0400	-0.0200	-
2	IC (AC)	0.9561	-0.0523	0.0230	0.0096	-
3	DC DG	0.9651	-	-	-	0.0204
4	DC DG	0.9643	-	-	-	0.0027
5	DC Load	0.9638	-	-	-	-0.0092
6	AC DG	0.9598	-0.0290	0.0132	0.0066	-
7	AC Load	0.9593	-0.0293	-0.0205	-0.0060	-
8	AC DG	0.9597	0.0003	0.0373	0.0151	-
9	AC Load	0.9593	-0.0118	-0.0298	-0.0070	-
10	IC (AC)	0.9598	0.0208	0.0169	0.0019	-

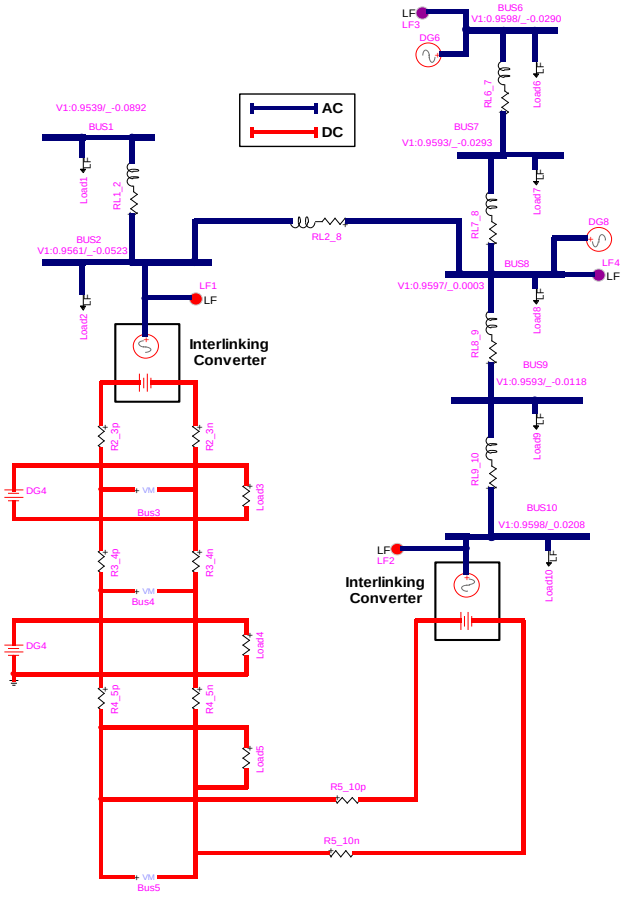

Figure 4.6 10-bus islanded AC/DC system ($Test\_3$) schematic in EMTP

4.2 Comparison of Load-Flow Methods for Islanded AC/DC Systems

In this section, both decoupled and generalized AC/DC load-flow methods are applied on an islanded AC/DC test system and they are compared in terms of performance.

4.2.1 Case Study

In order to compare the decoupled and generalized AC/DC load-flow methods, they must be applied on one test case and with utilization of one solution method (e.g. Newton). Therefore, an islanded 12-bus AC/DC system ($Test\_4$) is chosen for this comparison (Figure 4.7). The parameters of $Test\_4$ system such as impedances, loads, DGs and converter are derived from test systems mentioned in previous section and stated in Table 4.17, Table 4.18, and Table 4.19. The base values (apparent power, AC and DC voltages) for p.u. conversion are $S_{base} = 10\ MVA$, $V_{base}^{ac} = 4.16\ kV$, and $V_{base}^{dc} = 6.8\ kV$. Moreover, the acceptable voltage and frequency range for the system are $\pm 5\%$ and $\pm 1\%$, respectively. This system comprises two 6-bus AC and DC microgrids which are connected to each other via an interlinking converter. The efficiency, power factor, and the modulation index of the converter are $\eta_c = 98\%$, $\cos\varphi_c = 0.95$, and $M = 0.991$, respectively.

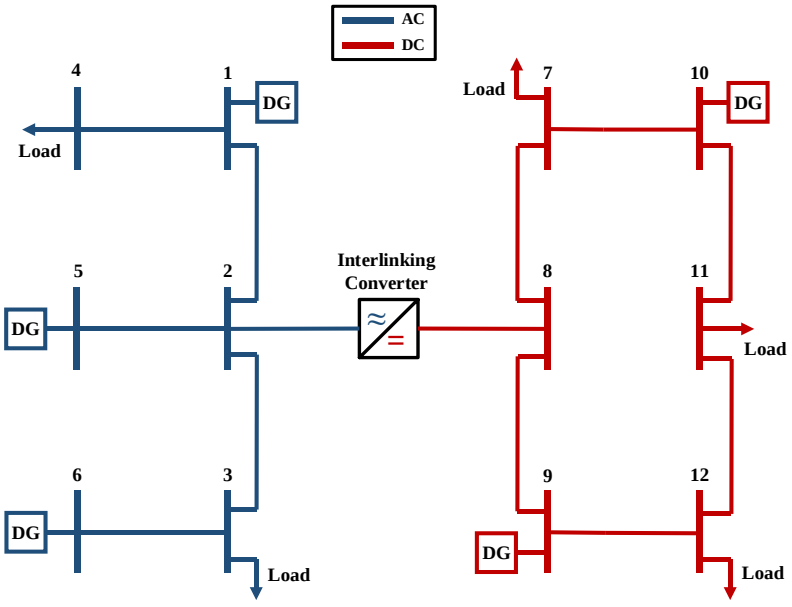

Figure 4.7 Islanded 12-bus AC/DC system ($Test\_4$) for comparison of load-flow methods

Table 4.17 Impedances of $Test\_4$ system

From Bus	To Bus	Resistance (Ω)	Inductance (Ω)
1	2	0.2218	0.3630
2	3	0.2218	0.3630
3	6	0.4435	0.7260
4	1	0.3105	0.3619
5	2	0.8870	1.4520
7	8	0.2208	-
8	9	0.4415	-
7	10	0.8830	-
9	12	0.8830	-
10	11	0.4415	-
11	12	0.2208	-

Table 4.18 Load data of $Test\_4$ system

Bus	$P_L^{ac}(MW)$	$Q_L^{ac}(MVAr)$	$P_L^{dc}(MW)$
3	0.4	0.2	-
4	0.4	0.2	-
7	-	-	0.1
11	-	-	0.1
12	-	-	0.1

Table 4.19 DGs and converter droop parameters of $Test\_4$ system

AC DGs	$\vartheta_{p_{ac}} = 0.16\ p.u.,\ \vartheta_{q_{ac}} = 2\ p.u.$
DC DGs	$\vartheta_{p_{dc}} = 1.333\ p.u.$
Converter (IC)	$\vartheta_{IC} = 10\ p.u.,\ \vartheta_{qIC} = 4\ p.u.$

The decoupled and generalized AC/DC load-flow algorithms are programed in MATLAB using Newton method ($Codes\ Package\backslash Comparison\backslash Case\ study\ with\ Decoupled\ method\backslash Test\_4\_D.m$ and $Codes\ Package\backslash Comparison\backslash Case\ study\ with\ Generalized\ method\backslash Test\_4\_G.m$) for the $Test\_4$ system and their results are compared in Table 4.20 and Table 4.21.

Table 4.20 Load-flow results of decoupled and generalized methods for $Test\_4$ system (voltages)

Bus	**Bus Type**	**Decoupled Method**		**Generalized Method**	
		$\boldsymbol{V}$ $(\boldsymbol{p.u.})$	$\boldsymbol{\delta}$ (°)	$\boldsymbol{V}$ $(\boldsymbol{p.u.})$	$\boldsymbol{\delta}$ (°)
1	AC DG	0.9667	0	0.9670	0
2	IC (AC)	0.9693	0.1448	0.9697	0.1447
3	AC Load	0.9656	0.0433	0.9659	0.0430
4	AC Load	0.9548	-0.2965	0.9551	-0.2963
5	AC DG	0.9881	1.3063	0.9883	1.3042
6	AC DG	0.9774	0.5496	0.9776	0.5485
7	DC Load	0.9786	-	0.9782	-
8	IC (DC)	0.9789	-	0.9785	-
9	DC DG	0.9796	-	0.9792	-
10	DC DG	0.9793	-	0.9789	-
11	DC Load	0.9782	-	0.9777	-
12	DC Load	0.9781	-	0.9776	-
Frequency (Hz)		59.7429		59.7438	

Table 4.21 Load-flow results of decoupled and generalized methods for $Test\_4$ system (powers)

Bus	**Decoupled Method**			**Generalized Method**		
	$\boldsymbol{P_{ac}}$ $(\boldsymbol{p.u.})$	$\boldsymbol{Q_{ac}}$ $(\boldsymbol{p.u.})$	$\boldsymbol{P_{dc}}$ $(\boldsymbol{p.u.})$	$\boldsymbol{P_{ac}}$ $(\boldsymbol{p.u.})$	$\boldsymbol{Q_{ac}}$ $(\boldsymbol{p.u.})$	$\boldsymbol{P_{dc}}$ $(\boldsymbol{p.u.})$
1	0.0268	0.0167	-	0.0267	0.0165	-
2	-0.0007	0.0077	-	-0.0003	0.0076	-
3	-0.0400	-0.0200	-	-0.0400	-0.0200	-
4	-0.0400	-0.0200	-	-0.0400	-0.0200	-
5	0.0268	0.0060	-	0.0267	0.0059	-
6	0.0268	0.0113	-	0.0267	0.0112	-
7	-	-	-0.0100	-	-	-0.0100
8	-	-	0.0007	-	-	-0.0000
9	-	-	0.0153	-	-	0.0156
10	-	-	0.0155	-	-	0.0158
11	-	-	-0.0100	-	-	-0.0100
12	-	-	-0.0100	-	-	-0.0100

It can be seen that the load-flow results (AC voltage magnitudes and phase angles, DC voltages, frequency, and AC and DC powers) of two methods are almost equal to each other. The slight differences are due to the different modeling approaches. For instance, in contrast with the decoupled modeling approach, in unified approach, some extra parameters such as efficiency, power factor, and modulation index are considered for the interlinking converter.

4.2.2 Performance Comparison

In 4.2.1, the load-flow results of both decoupled and generalized methods have been compared to each other as shown in Table 4.20. In this section, their performances are compared to each other. This includes the average required computational time for the computer with "Intel Core i7-7700 HQ @ 2.80 GHz CPU and 32 GB RAM" and the number of iterations needed for convergence of load-flow algorithms.

Table 4.22 presents the performance parameters of decoupled and generalized load-flow methods for the 12-bus AC/DC $Test\_4$ system shown in Figure 4.7 and with the pre-defined maximum mismatch of 10^{-6}.

Table 4.22 Performance comparison of decoupled and generalized load-flow methods

	Decoupled Method	**Generalized Method**
Number of Iterations	306	125
Avg. Computational Time (s)	0.189	0.298

It can be seen that for such a small islanded AC/DC system (12-bus), the number of iterations for both load-flow methods are relatively high. This high number of iterations might result in divergence for larger AC/DC systems. As mentioned in section 4.1.1, the reason could be the variable frequency and its impact on admittances and voltages. The other reason could be the lower X/R ratio in low- or medium-voltage. This might cause a larger number of iterations that Newton load-flow algorithm required for convergence [117]. This idea is tested on $Test\_4$ system by increasing the inductances of its AC lines and running the load-flow algorithms. It is observed that by increasing the AC line inductances the number of iterations required for convergence in decoupled and generalized load-flow algorithm are reduced. In order to discover which parameters

are responsible for the large number of iterations, two tests have been accomplished for both load-flow methods.

4.2.2.1 Iteration Tests for Decoupled Load-flow Method

First, by employing the final results of the load-flow problem, it is found out that even if all the parameters except AC voltages are known, the number of iterations does not change. However, if we consider that the AC voltages are known variables (using final values of AC voltages from Table 4.20 in decoupled load-flow algorithm and not updating them in each iteration), the algorithm solves the problem for other unknowns and it converges in only 10 iterations instead of 306. In addition, the average computational time is reduced to "0.011 *s*" from "0.189 *s*". This clearly shows that large number of iterations is caused by AC voltages calculation in load-flow problem.

Second, the parameters are plotted with respect to the number of iterations to see their trends during the iterations. As shown in Figure 4.8, it can also be seen that in contrast to DC voltages, frequency and phase angles, the AC voltage magnitudes reach their final values quite slowly. This confirms the outcome of first test which shows the link between large number of iterations and calculation of AC voltages in decoupled AC/DC load-flow solution method.

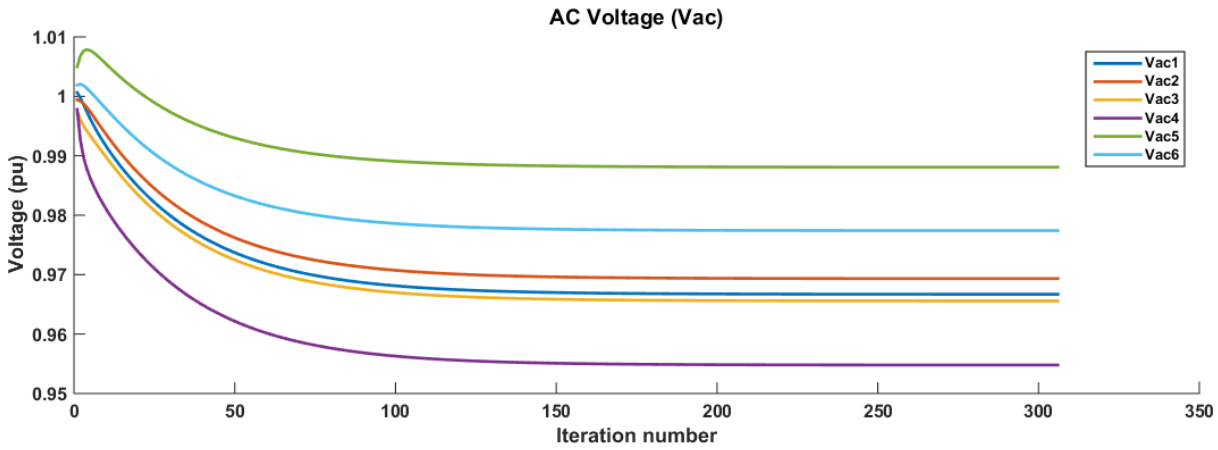

Figure 4.8: Decoupled load-flow parameters with respect to number of iterations

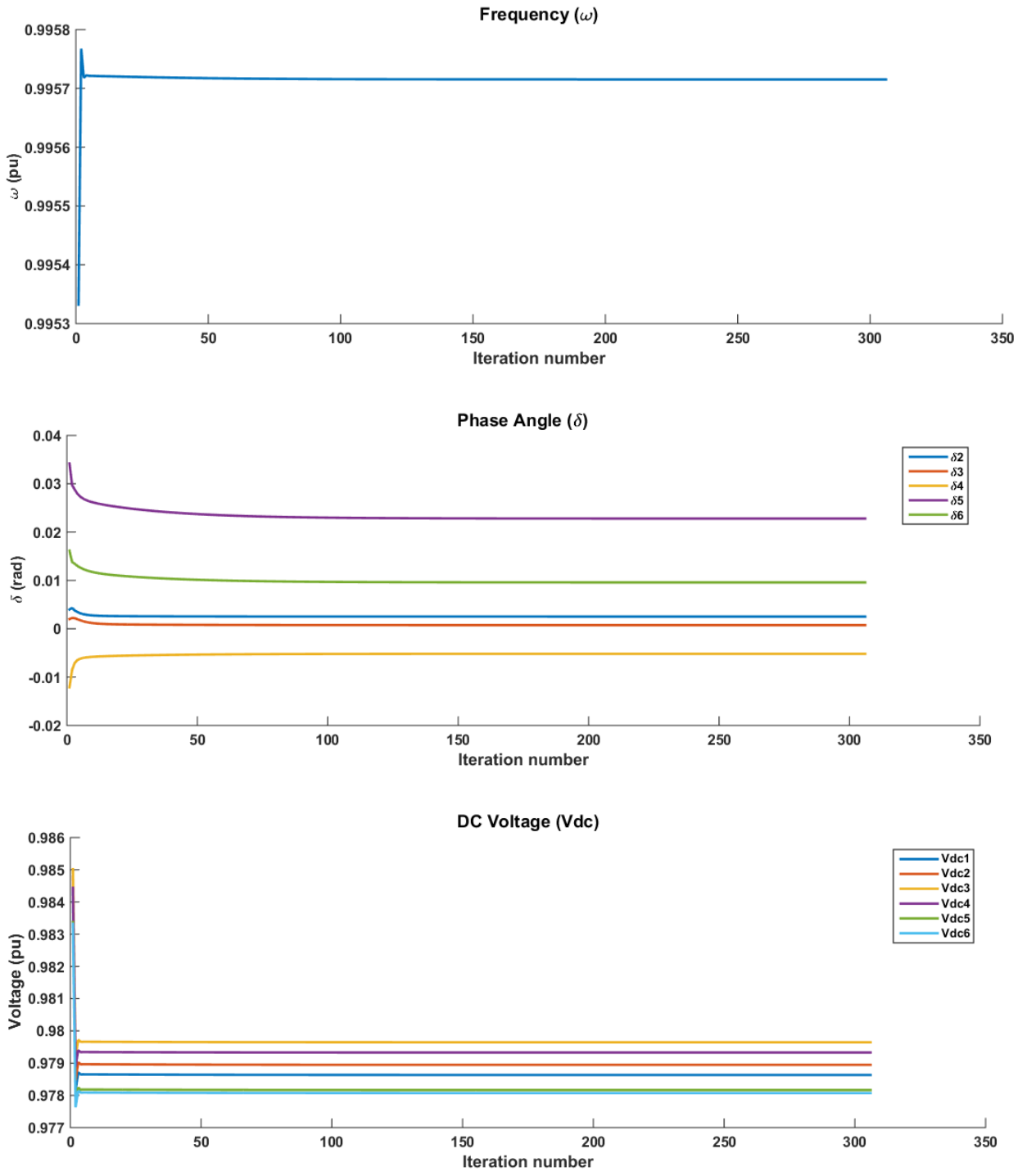

Figure 4.8 Decoupled load-flow parameters with respect to number of iterations (continued)

4.2.2.2 Iteration Tests for Generalized Load-flow Method

By performing the aforementioned tests on generalized load-flow algorithm, it can be seen that the voltages are the reason for higher number of iterations in an islanded AC/DC system compared to a grid-connected case. Since in this method AC and DC parts are modeled together as a unified system, both AC and DC voltages must be considered as a unique vector and the test should be done with respect to this assumption. In this case, it is found out that if the voltages are known variables (using final values of voltages from Table 4.20 in generalized load-flow algorithm and not updating them in each iteration), the load-flow problem converges after only 11 iterations instead of 125 iterations and the average computational time of the algorithm reduced from "0.292 *s*" to "0.033 *s*". This clearly indicates that the reason for such a relatively large number of iterations is due to the calculation of voltages.

Moreover, as presented in Figure 4.9, it can be noticed that compared to the other parameters, voltages (both AC and DC) require more iterations to reach their final values. This confirms the outcome of first test which shows the link between large number of iterations and calculation of voltages in generalized AC/DC load-flow solution method for islanded systems.

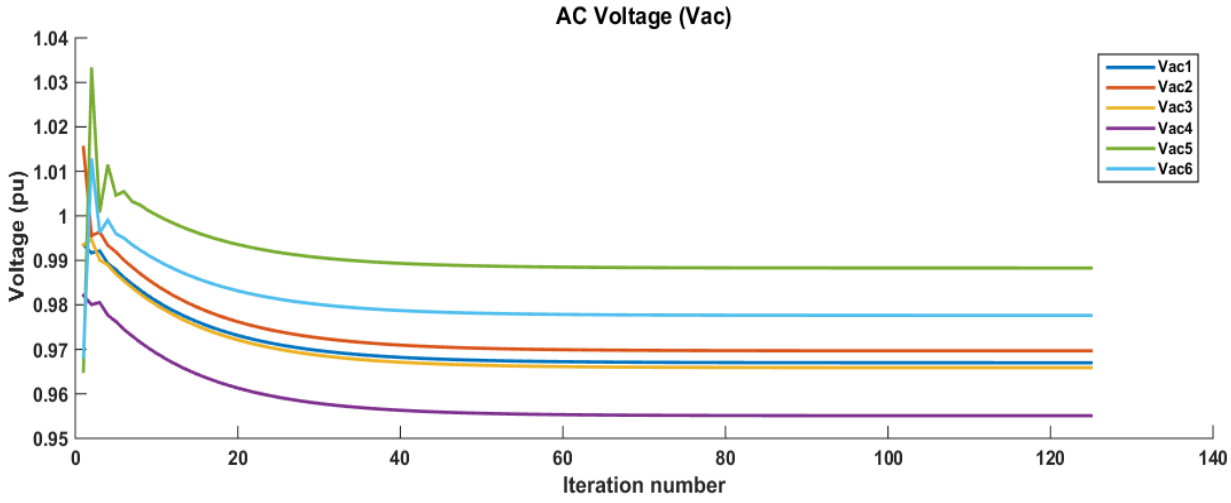

Figure 4.9 Generalized load-flow parameters with respect to number of iterations

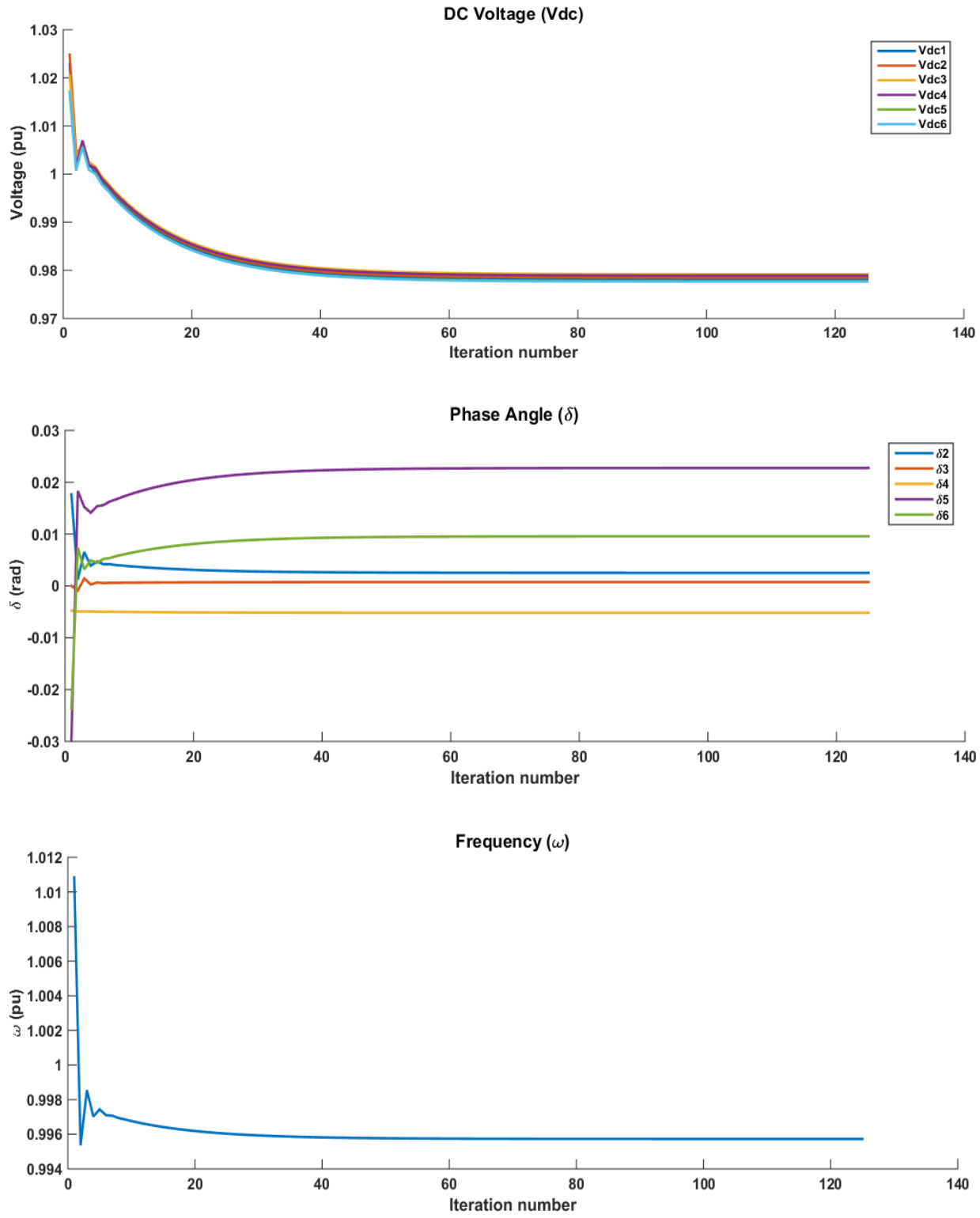

Figure 4.9 Generalized load-flow parameters with respect to number of iterations (continued)

4.3 Improvement of Load-Flow Algorithms for Islanded AC/DC Systems

In this section, in order to improve the performance (i.e. accelerate the algorithm) of the decoupled and generalized AC/DC load-flow algorithms, two improvement techniques are firstly introduced in 4.3.1 and then in 4.3.2 applied on the load-flow algorithms of the previous 12-bus system case study.

4.3.1 Load-Flow Performance Improvement Techniques

In order to accelerate the decoupled and generalized load-flow algorithms which are solved based on Newton method, two improvement techniques can be employed.

The first technique is to utilize the steady-state results of the simplified system instead of the flat start ($V^{(0)} = 1.0\, p.u.$ and $\delta^{(0)} = 0.0°$) approach as initial values for the load-flow algorithm. To find the steady-state solution for a simplified system, it should be assumed that the DG and IC buses have voltage magnitudes of $V = 1.0\, p.u.$ and phase angles of $\delta = 0.0°$. By simulating this simplified version of the AC/DC system in a time-domain simulation tool such as EMTP, the steady-state results (voltage magnitudes and phase angles) for load buses can be utilized as load-flow initial values for those buses. Since these initial values are closer to final load-flow results, the steady-state initialization would accelerate the load-flow algorithm and reduce the number of iterations required for its convergence. However, the time required to find the steady-state solution of the simplified system must be considered.

The other technique to accelerate the algorithms and reduce the number of iterations is to utilize percentage (or p.u.) tolerance or mismatch [121]. In this approach, the mismatch value at each iteration is determined in a different way. In conventional Newton method, the updating vector and updating equation are:

$$\Delta x^{(k)} = -J^{-1(k)} f(x^{(k)}) \tag{4.1}$$

$$x^{(k+1)} = x^{(k)} + \Delta x^{(k)} \tag{4.2}$$

Where,"k" is number of iterations, $f\left(x^{(k)}\right)$ is the vector of mismatch equations at "k^{th}" iteration, J is the Jacobian matrix, and $x^{(k)}$ is the vector of unknown values at "k^{th}" iteration. The mismatch in each iteration is determined as the maximum value of $\left|f\left(x^{(k)}\right)\right|$ or maximum value of $\left|\Delta x^{(k)}\right|$. The algorithm

continues to iterate until the mismatch value is smaller than a pre-defined value (tolerance or maximum mismatch ε):

$$max\left(\left|\Delta x^{(k)}\right|\right) \leq \varepsilon \tag{4.3}$$

If the percentage tolerance is considered, in order to check the convergence criteria, the mismatch in each iteration is calculated by dividing updating vector over unknown variable vector as follows [121]:

$$max\left(\frac{\left|\Delta x^{(k)}\right|}{\left|x^{(k+1)}\right|}\right) \leq \varepsilon \tag{4.4}$$

In this case, larger pre-defined tolerance can be used which leads to faster convergence of the load-flow algorithm with lower number of iterations. For instance, if the tolerance is equal to 10^{-6} with normal mismatch calculation, in case of percentage mismatch calculation, the tolerance could be increased to 10^{-4} or 10^{-3} without having any impact on the accuracy of load-flow results and the algorithm converges faster within lower number of iterations.

4.3.2 Improvement of Load-flow Algorithms

To verify the effectiveness of mentioned improvement techniques, they are applied into decoupled and generalized load-flow algorithms and the obtained results for the $Test\_4$ system (Figure 4.7) are compared to ones stated in Table 4.22.

By employing the steady-state initialization technique in both decoupled and generalized load-flow algorithms for $Test\_4$ system, it can be seen that it does not have a considerable impact on generalized method and it has only a negligible impact on decoupled method as it reduces the number of iterations from 306 to 294, and the average computational time from $0.189\,s$ to $0.178\,s$. As expected, this technique does not affect the accuracy of algorithms as the load-flow results obtained after applying this technique are completely equal to ones stated in Table 4.20. The impact of applying steady-state initialization technique on load-flow performances are shown in Table 4.23.

Table 4.23 Impact of steady-state initialization on performance of load-flow methods

	Decoupled Method	**Generalized Method**
Number of Iterations	294	125
Avg. Computational Time (s)	0.178	0.292

However, the percentage tolerance technique has more impact on performance of both load-flow methods. Table 4.24 presents the number of iterations and the average computational time required for both load-flow methods to converge by using percentage tolerance calculation and with pre-defined maximum mismatch of 10^{-4} for the $Test\_4$ system shown in Figure 4.7. It can be seen that using the percentage tolerance in the load-flow algorithms can result in significant decrease in number of iterations and computational time without having a considerable impact on load-flow results. For decoupled method, the number of iterations is almost halved, (reduced from 306 to 151) and the average computational time is decreased from $0.178\,s$ to $0.094\,s$. For generalized method, the number of iterations and the average computational time are reduced from 125 to 86, and $0.298\,s$ to $0.210\,s$, respectively. The accuracy analysis is also performed for percentage tolerance calculation by comparing the load-flow results using this technique with the results using normal tolerance calculation shown in Table 4.20. As indicated by Table 4.25, it is noticed that using percentage tolerance technique with maximum pre-defined mismatch of 10^{-4} instead of 10^{-6} for normal tolerance calculation, does not have a considerable impact on accuracy of both load-flow results.

Finally, it is also possible to apply both improvement techniques at the same time for the decoupled and generalized load-flow methods. This is done by using the steady-state initialization results as the initial value for the load-flow algorithms, in addition to calculating the mismatch by percentage tolerance approach. However, as expected, the results do not have much difference with the previous approach (percentage tolerance) as the steady-state initialization does not have a significant impact on the performance of the load-flow algorithms (as shown in Table 4.23). Table 4.26 summarizes the impact of applying both improvement techniques on decoupled and generalized load-flow algorithms for $Test\_4$ system. As mentioned before, steady-state initialization technique does not affect the accuracy of the algorithms. Hence, the load-flow results after applying both improvement techniques are completely identical to results when only percentage tolerance technique is applied (Table 4.25).

Table 4.24 Impact of percentage tolerance calculation on performance of load-flow methods

	Decoupled Method	**Generalized Method**
Number of Iterations	151	86
Avg. Computational Time (s)	0.094	0.210

Table 4.25 Comparison of load-flow results for $Test\_4$ system with and without using percentage tolerance calculation technique

Bus	**Decoupled Method**				**Generalized Method**			
	Normal Tolerance		**Percentage Tolerance**		**Normal Tolerance**		**Percentage Tolerance**	
	$\boldsymbol{V}$ $(\boldsymbol{p.u.})$	$\boldsymbol{\delta}$ (°)	$\boldsymbol{V}$ $(\boldsymbol{p.u.})$	$\boldsymbol{\delta}$ (°)	$\boldsymbol{V}$ $(\boldsymbol{p.u.})$	$\boldsymbol{\delta}$ (°)	$\boldsymbol{V}$ $(\boldsymbol{p.u.})$	$\boldsymbol{\delta}$ (°)
1	0.9667	0	0.9670	0	0.9670	0	0.9670	0
2	0.9693	0.1448	0.9696	0.1449	0.9697	0.1447	0.9697	0.1448
3	0.9656	0.0433	0.9659	0.0434	0.9659	0.0430	0.9659	0.0430
4	0.9548	-0.2965	0.9551	-0.2969	0.9551	-0.2963	0.9551	-0.2963
5	0.9881	1.3063	0.9883	1.3085	0.9883	1.3042	0.9883	1.3035
6	0.9774	0.5496	0.9776	0.5509	0.9776	0.5485	0.9777	0.5481
7	0.9786	-	0.9786	-	0.9782	-	0.9782	-
8	0.9789	-	0.9789	-	0.9785	-	0.9785	-
9	0.9796	-	0.9796	-	0.9792	-	0.9792	-
10	0.9793	-	0.9793	-	0.9789	-	0.9789	-
11	0.9782	-	0.9782	-	0.9777	-	0.9778	-
12	0.9781	-	0.9781	-	0.9776	-	0.9777	-
f (Hz)	59.7429		59.7429		59.7438		59.7439	

Table 4.26 Impact of both improvement techniques on performance of load-flow methods

	Decoupled Method	**Generalized Method**
Number of Iterations	138	85
Avg. Computational Time (s)	0.085	0.207

Based on the results stated in Table 4.23, Table 4.24, and Table 4.26, it can be concluded that both improvement techniques can enhance the performance of decoupled and generalized load-flow algorithms. However, percentage tolerance technique is simpler to implement as it does not require additional calculation like steady-state initialization. It is also more effective than steady-state initialization on performance of load-flow algorithms as it results in faster convergence with lower number of iterations. This reduces the risk of divergence in load-flow solution of larger systems. Nevertheless, the number of iterations in both load-flow algorithms is still quite large for such a small islanded AC/DC system and this might result in divergence for larger systems.

CHAPTER 5 CONCLUSION

In this chapter, at first, a summary of the research accomplished in this thesis is presented. Furthermore, recommendations for future research work are highlighted.

5.1 Summary

AC/DC distribution systems offer several advantages such as loss reduction compared to conventional AC distribution systems. In order to make them operational, several power systems studies must be performed, among which load-flow is the most fundamental one. The primary objective of this thesis is to comprehensively review the load-flow methods for AC/DC power systems especially at distribution level. This includes AC/DC system modeling approaches, solution procedures utilized for load-flow analysis, and the performance of AC/DC load-flow methods proposed in the literature. Moreover, the effectiveness and the accuracy of two recently proposed load-flow methods for AC/DC distribution systems operating in grid-connected and islanded modes are validated by comparing their results with steady-state results obtained by a time-domain simulation software (EMTP). Afterwards, the selected AC/DC load-flow methods are compared to each other in terms of their algorithm performances (number of iterations required to reach convergence and average computational time needed for each algorithm to solve the load-flow problem) by applying them on an islanded test AC/DC system. Finally, in order to enhance their efficiency (reducing number of iterations and average computational time) two improvement techniques (steady-state initialization of system and calculating the mismatch in each iteration using percentage tolerance method) are introduced and applied. Although these techniques can improve the efficiency of selected load-flow methods for islanded systems, but this improvement is still not completely sufficient as the number of iterations required for algorithms' convergence is still quite large compared to one for grid-connected systems. Therefore, this issue must be addressed in future research work.

5.2 Directions for Future Work

As mentioned above, despite applying two improvement techniques, there is still lack of efficiency (a large number of iterations required for convergence) in both decoupled and generalized AC/DC load-flow methods when utilized for islanded systems. Furthermore, these load-flow methods are

only applicable for balanced AC/DC systems with limited types of components. For instance, only AC/DC converters are considered in theses load-flow methods and other types such as DC/DC converters are not taken into account. Moreover, as stated in 3.1.1.3, several control modes such as constant active or reactive powers, and constant AC or DC voltages can be included in modeling of AC/DC converters for load-flow analysis. However, they are not included in decoupled and generalized load-flow methods. To the best of the author knowledge, there is still no AC/DC load-flow method proposed in the literature which is applicable to be utilized for any types of AC/DC systems (grid-connected and islanded) without the above-mentioned limitations. An appropriate example for such comprehensive load-flow method is MANA which now is only utilized for AC systems. But, as a multi-phase load-flow method which can include any types of components' equations, MANA has the potential to be expanded for any types of AC/DC systems with any types of power converters. In addition, by using MANA load-flow solution a precise time-domain initialization can be provided in EMTP [10]. Therefore, the following tasks are suggested for future load-flow methods of AC/DC distribution systems:

- Comprehensive modeling of AC/DC distribution systems (grid-connected or islanded) including converters with different control modes, and various AC and DC DGs and loads for load-flow analysis.
- Expanding MANA AC load-flow approach to formulate a generic multi-phase AC/DC load-flow method which considers unbalances in the system as well as the aforementioned constraints.

REFERENCES

[1] I. R. E. A. (IRENA), "Future of Solar Photovoltaic: Deployment, investment, technology, grid integration and socio-economic aspects (A Global Energy Transformation: paper)," International Renewable Energy Agency, Abu Dhabi2019.

[2] I. R. E. A. (IRENA), "Battery Storage for Renewables: Market Status and Technology Outlook," 2015, Available: http://www.irena.org/publications/2015/Jan/Battery-Storage-for-Renewables-Market-Status-and-Technology-Outlook.

[3] I. E. A. (IEA), "Global EV Outlook 2018," 2018, Available: https://webstore.iea.org/global-ev-outlook-2018.

[4] W. Peng, L. Goel, L. Xiong, and C. Fook Hoong, "Harmonizing AC and DC: A Hybrid AC/DC Future Grid Solution," *IEEE Power and Energy Magazine*, vol. 11, no. 3, pp. 76-83, 2013.

[5] K. Kurohane, T. Senjyu, A. Yona, N. Urasaki, T. Goya, and T. Funabashi, "A Hybrid Smart AC/DC Power System," *IEEE Transactions on Smart Grid*, vol. 1, no. 2, pp. 199-204, 2010.

[6] S. K. Chaudhary, J. M. Guerrero, and R. Teodorescu, "Enhancing the Capacity of the AC Distribution System Using DC Interlinks—A Step Toward Future DC Grid," *IEEE Transactions on Smart Grid*, vol. 6, no. 4, pp. 1722-1729, 2015.

[7] M. Starke, L. M. Tolbert, and B. Ozpineci, "AC vs. DC distribution: A loss comparison," pp. 1-7, 2008.

[8] N. Eghtedarpour and E. Farjah, "Power Control and Management in a Hybrid AC/DC Microgrid," (in English), *Ieee Transactions on Smart Grid*, vol. 5, no. 3, pp. 1494-1505, May 2014.

[9] J. J. Grainger and W. D. Stevenson, *Power system analysis*. McGraw-Hill, 1994.

[10] J. Mahseredjian, S. Dennetiere, L. Dube, B. Khodabakhchian, and L. Gerin-Lajoie, "On a new approach for the simulation of transients in power systems," (in English), *Electric Power Systems Research*, vol. 77, no. 11, pp. 1514-1520, Sep 2007.

[11] A. P. Technologies, *It's Time to Connect: Technical Description of HVDC Light Technology*. ABB Power Technologies AB, 2005.

[12] P. Wang, J. Xiao, C. Jin, X. Han, and W. Qin, "Hybrid AC/DC Micro-Grids: Solution for High Efficient Future Power Systems," in *Sustainable Power Systems: Modelling, Simulation and Analysis*, N. R. Karki, R. Karki, A. K. Verma, and J. Choi, Eds. Singapore: Springer Singapore, 2017, pp. 23-40.

[13] L. Zhang, F. Gao, N. Li, Q. Zhang, and C. Wang, "Interlinking modular multilevel converter of hybrid AC-DC distribution system with integrated battery energy storage," pp. 70-77, 2015.

[14] C. Qi *et al.*, "A Decentralized Optimal Operation of AC/DC Hybrid Distribution Grids," *IEEE Transactions on Smart Grid*, pp. 1-1, 2017.

[15] E. Unamuno and J. A. Barrena, "Hybrid ac/dc microgrids—Part I: Review and classification of topologies," *Renewable and Sustainable Energy Reviews*, vol. 52, pp. 1251-1259, 2015.

[16] S. Europe, "Global Market Outlook for Solar Power 2016-2020," 2016, Available: http://www.solarpowereurope.org/reports/global-market-outlook-2017/.

[17] Z. Weichao, L. Haifeng, B. Zhou, L. Wei, and G. Ran, "Review of DC technology in future smart distribution grid," pp. 1-4, 2012.

[18] P. Zhang, F. Yan, and C. Du, "A comprehensive analysis of energy management strategies for hybrid electric vehicles based on bibliometrics," *Renewable and Sustainable Energy Reviews*, vol. 48, pp. 88-104, 2015.

[19] C. Deng, N. Liang, J. Tan, and G. Wang, "Multi-Objective Scheduling of Electric Vehicles in Smart Distribution Network," *Sustainability*, vol. 8, no. 12, p. 1234, 2016.

[20] B. Kroposki, "Integrating high levels of variable renewable energy into electric power systems," *Journal of Modern Power Systems and Clean Energy*, vol. 5, no. 6, pp. 831-837, 2017.

[21] M. S. ElNozahy and M. M. A. Salama, "A Comprehensive Study of the Impacts of PHEVs on Residential Distribution Networks," *IEEE Transactions on Sustainable Energy*, vol. 5, no. 1, pp. 332-342, 2014.

[22] E. Unamuno and J. A. Barrena, "Hybrid ac/dc microgrids—Part II: Review and classification of control strategies," *Renewable and Sustainable Energy Reviews*, vol. 52, pp. 1123-1134, 2015.

[23] B. Stott, "Review of load-flow calculation methods," *Proceedings of the IEEE*, vol. 62, no. 7, pp. 916-929, 1974.

[24] J. D. Glover, M. S. Sarma, and T. Overbye, *Power System Analysis and Design*. Cengage Learning, 2011.

[25] I. Kocar, J. Mahseredjian, U. Karaagac, G. Soykan, and O. Saad, "Multiphase Load-Flow Solution for Large-Scale Distribution Systems Using MANA," *IEEE Transactions on Power Delivery*, vol. 29, no. 2, pp. 908-915, 2014.

[26] A. G. Exposito and E. R. Ramos, "Augmented rectangular load flow model," *IEEE Transactions on Power Systems*, vol. 17, no. 2, pp. 271-276, 2002.

[27] J. Arrillaga and P. Bodger, "Integration of h.v.d.c. links with fast-decoupled load-flow solutions," *Proceedings of the Institution of Electrical Engineers*, vol. 124, no. 5, p. 463, 1977.

[28] J. Reeve, G. Fahny, and B. Stott, "Versatile load flow method for multiterminal HVDC systems," *IEEE Transactions on Power Apparatus and Systems*, vol. 96, no. 3, pp. 925-933, 1977.

[29] J. Beerten, S. Cole, and R. Belmans, "A sequential AC/DC power flow algorithm for networks containing Multi-terminal VSC HVDC systems," pp. 1-7, 2010.

[30] M. Baradar and M. Ghandhari, "A Multi-Option Unified Power Flow Approach for Hybrid AC/DC Grids Incorporating Multi-Terminal VSC-HVDC," *IEEE Transactions on Power Systems,* vol. 28, no. 3, pp. 2376-2383, 2013.

[31] Y. Gao, S. Li, W. Dong, and B. Lu, "Decoupled AC/DC Power Flow Strategy for Multiterminal HVDC Systems," *International Journal of Emerging Electric Power Systems,* vol. 19, no. 1, 2018.

[32] W. Wang and M. Barnes, "Power Flow Algorithms for Multi-Terminal VSC-HVDC With Droop Control," *IEEE Transactions on Power Systems,* vol. 29, no. 4, pp. 1721-1730, 2014.

[33] J. Lei, T. An, Z. Du, and Z. Yuan, "A General Unified AC/DC Power Flow Algorithm With MTDC," *IEEE Transactions on Power Systems,* vol. 32, no. 4, pp. 2837-2846, 2017.

[34] H. M. A. Ahmed, A. B. Eltantawy, and M. M. A. Salama, "A Generalized Approach to the Load Flow Analysis of AC–DC Hybrid Distribution Systems," *IEEE Transactions on Power Systems,* vol. 33, no. 2, pp. 2117-2127, 2018.

[35] M. Khan, S. Jamali, C.-H. Noh, G.-H. Gwon, and C.-H. Kim, "A Load Flow Analysis for AC/DC Hybrid Distribution Network Incorporated with Distributed Energy Resources for Different Grid Scenarios," *Energies,* vol. 11, no. 2, p. 367, 2018.

[36] H. Liang, X. Zhao, X. Yu, Y. Gao, and J. Yang, "Study of Power Flow Algorithm of AC/DC Distribution System including VSC-MTDC," *Energies,* vol. 8, no. 8, pp. 8391-8405, 2015.

[37] E. Aprilia, K. Meng, M. Al Hosani, H. H. Zeineldin, and Z. Y. Dong, "Unified Power Flow Algorithm for Standalone AC/DC Hybrid Microgrids," *IEEE Transactions on Smart Grid,* vol. 10, no. 1, pp. 639-649, 2019.

[38] A. A. Eajal, M. A. Abdelwahed, E. F. El-Saadany, and K. Ponnambalam, "A Unified Approach to the Power Flow Analysis of AC/DC Hybrid Microgrids," *IEEE Transactions on Sustainable Energy,* vol. 7, no. 3, pp. 1145-1158, 2016.

[39] A. A. Hamad, M. A. Azzouz, and E. F. El Saadany, "A Sequential Power Flow Algorithm for Islanded Hybrid AC/DC Microgrids," *IEEE Transactions on Power Systems,* vol. 31, no. 5, pp. 3961-3970, 2016.

[40] M. A. Allam, A. A. Hamad, and M. Kazerani, "A Sequence-Component-Based Power-Flow Analysis for Unbalanced Droop-Controlled Hybrid AC/DC Microgrids," (in English), *Ieee Transactions on Sustainable Energy,* vol. 10, no. 3, pp. 1248-1261, Jul 2019.

[41] Y. Xiao, C. G. Ren, X. Q. Han, and P. Wang, "A Generalized and Mode-Adaptive Approach to the Power Flow Analysis of the Isolated Hybrid AC/DC Microgrids," (in English), *Energies,* vol. 12, no. 12, Jun 2 2019.

[42] J. Beerten, S. Cole, and R. Belmans, "Generalized Steady-State VSC MTDC Model for Sequential AC/DC Power Flow Algorithms," *IEEE Transactions on Power Systems,* vol. 27, no. 2, pp. 821-829, 2012.

[43] M. Baradar, M. Ghandhari, and D. Van Hertem, "The modeling multi-terminal VSC-HVDC in power flow calculation using unified methodology," pp. 1-6, 2011.

[44] C. Liu, B. Zhang, Y. Hou, F. F. Wu, and Y. Liu, "An Improved Approach for AC-DC Power Flow Calculation With Multi-Infeed DC Systems," *IEEE Transactions on Power Systems,* vol. 26, no. 2, pp. 862-869, 2011.

[45] M. El-marsafawy and R. Mathur, "A New, Fast Technique for Load-Flow Solution of Integrated Multi-Terminal DC/AC Systems," *IEEE Transactions on Power Apparatus and Systems*, vol. PAS-99, no. 1, pp. 246-255, 1980.

[46] J.-C. Fernandez-Perez, F. M. Echavarren Cerezo, and L. R. Rodriguez, "On the Convergence of the Sequential Power Flow for Multiterminal VSC AC/DC Systems," *IEEE Transactions on Power Systems*, vol. 33, no. 2, pp. 1768-1776, 2018.

[47] S. Z. M. Omer. Khan, M. Mehdi, J. Han, G.H. Gwon, C.H. Noh, J.I. Song, C.H. Kim, "Load flow analysis for DER integrated AC/DC distribution system affected by converter and DC line outages," in *International Conference on Power Systems Transients (IPST2017)*, Seoul, Republic of Korea, 2017.

[48] M. Z. Kamh and R. Iravani, "A Unified Three-Phase Power-Flow Analysis Model For Electronically Coupled Distributed Energy Resources," *IEEE Transactions on Power Delivery*, vol. 26, no. 2, pp. 899-909, 2011.

[49] F. YalÇIn and U. ArİFoĞLu, "A new sequential power flow algorithm for AC/DC systems including independent multiterminal DC subsystems," *Turkish Journal of Electrical Engineering & Computer Sciences*, vol. 25, pp. 3097-3112, 2017.

[50] M. E. Nassar, A. A. Hamad, M. M. A. Salama, and E. F. El-Saadany, "A Novel Load Flow Algorithm for Islanded AC/DC Hybrid Microgrids," *IEEE Transactions on Smart Grid*, pp. 1-1, 2017.

[51] R. Chai, B. Zhang, J. Dou, Z. Hao, and T. Zheng, "Unified Power Flow Algorithm Based on the NR Method for Hybrid AC/DC Grids Incorporating VSCs," *IEEE Transactions on Power Systems*, vol. 31, no. 6, pp. 4310-4318, 2016.

[52] E. Acha, B. Kazemtabrizi, and L. M. Castro, "A New VSC-HVDC Model for Power Flows Using the Newton-Raphson Method," *IEEE Transactions on Power Systems*, vol. 28, no. 3, pp. 2602-2612, 2013.

[53] J. Beerten and R. Belmans, "Development of an open source power flow software for high voltage direct current grids and hybrid AC/DC systems: MATACDC," *IET Generation, Transmission & Distribution*, vol. 9, no. 10, pp. 966-974, 2015.

[54] S. H. D. Dhua, Q. Wu, "Load Flow Analysis of Hybrid AC-DC Power System with Offshore Wind Power," in *IEEE PES Innovative Smart Grid Technologies Asia*, Auckland, New Zealand, 2017.

[55] K. N. Narayanan and P. Mitra, "A comparative study of a sequential and simultaneous AC-DC power flow algorithms for a multi-terminal VSC-HVDC system," pp. 1-6, 2013.

[56] P. E. Wiernes, J. Priebe, S. Pleines, and A. Moser, "Performance comparision of integrated AC/DC power flow calculation methodologies," pp. 1-6, 2016.

[57] B. Muruganantham, R. Gnanadass, and N. P. Padhy, "Performance analysis and comparison of load flow methods in a practical distribution system," pp. 1-6, 2016.

[58] G. W. Stagg and A. H. El-Abiad, *Computer methods in power system analysis*. McGraw-Hill, 1968.

[59] J. Beerten, "Power flow modeling of hybrid AC/DC systems," in *HVDC Grids: For Offshore and Supergrid of the Future*, 2016.

[60] F. Mumtaz, M. H. Syed, M. A. Hosani, and H. H. Zeineldin, "A Novel Approach to Solve Power Flow for Islanded Microgrids Using Modified Newton Raphson With Droop Control of DG," *IEEE Transactions on Sustainable Energy,* vol. 7, no. 2, pp. 493-503, 2016.

[61] W. W. Price *et al.*, "Load Representation for Dynamic Performance Analysis," (in English), *Ieee Transactions on Power Systems,* vol. 8, no. 2, pp. 472-482, May 1993.

[62] J. M. Guerrero, M. Chandorkar, T.-L. Lee, and P. C. Loh, "Advanced Control Architectures for Intelligent Microgrids—Part I: Decentralized and Hierarchical Control," *IEEE Transactions on Industrial Electronics,* vol. 60, no. 4, pp. 1254-1262, 2013.

[63] N. Pogaku, M. Prodanovic, and T. C. Green, "Modeling, Analysis and Testing of Autonomous Operation of an Inverter-Based Microgrid," *IEEE Transactions on Power Electronics,* vol. 22, no. 2, pp. 613-625, 2007.

[64] X. Lu, K. Sun, J. M. Guerrero, J. C. Vasquez, and L. Huang, "State-of-Charge Balance Using Adaptive Droop Control for Distributed Energy Storage Systems in DC Microgrid Applications," *IEEE Transactions on Industrial Electronics,* vol. 61, no. 6, pp. 2804-2815, 2014.

[65] P. C. Loh and F. Blaabjerg, "Autonomous control of distributed storages in microgrids," pp. 536-542, 2011.

[66] B.-H. Kim, H. Kim, and B. Lee, "Parameter Estimation for the Composite Load Model," *Journal of International Council on Electrical Engineering,* vol. 2, no. 2, pp. 215-218, 2014.

[67] W. W. Price *et al.*, "Standard Load Models for Power-Flow and Dynamic Performance Simulation," (in English), *Ieee Transactions on Power Systems,* vol. 10, no. 3, pp. 1302-1313, Aug 1995.

[68] N. J. B. P. Kundur, and M. G. Lauby, *Power System Stability And Control*. McGraw-Hill, 1994.

[69] M. M. A. Abdelaziz, H. E. Farag, E. F. El-Saadany, and Y. A.-R. I. Mohamed, "A Novel and Generalized Three-Phase Power Flow Algorithm for Islanded Microgrids Using a Newton Trust Region Method," *IEEE Transactions on Power Systems,* vol. 28, no. 1, pp. 190-201, 2013.

[70] P. C. Loh, D. Li, Y. K. Chai, and F. Blaabjerg, "Autonomous Operation of Hybrid Microgrid With AC and DC Subgrids," *IEEE Transactions on Power Electronics,* vol. 28, no. 5, pp. 2214-2223, 2013.

[71] X. Zhang, X. Han, M. Yang, D. Sun, Y. Zhang, and W. Gai, "A Novel Power Flow Algorithm for Hybrid AC/DC Power Grids," *Electric Power Components and Systems,* vol. 45, no. 14, pp. 1607-1616, 2017.

[72] S. Cole, J. Beerten, and R. Belmans, "Generalized Dynamic VSC MTDC Model for Power System Stability Studies," *IEEE Transactions on Power Systems,* vol. 25, no. 3, pp. 1655-1662, 2010.

[73] K. R. Fleischer and R. S. Munnings, "Power systems analysis for direct current (DC) distribution systems," pp. 181-190, 1994.

[74] D. Salomonsson and A. Sannino, "Load modelling for steady-state and transient analysis of low-voltage DC systems," *IET Electric Power Applications,* vol. 1, no. 5, p. 690, 2007.

[75] A. Kwasinski and C. N. Onwuchekwa, "Dynamic Behavior and Stabilization of DC Microgrids With Instantaneous Constant-Power Loads," *IEEE Transactions on Power Electronics,* vol. 26, no. 3, pp. 822-834, 2011.

[76] L. Mackay, N. H. v. d. Blij, L. Ramirez-Elizondo, and P. Bauer, "Toward the Universal DC Distribution System," *Electric Power Components and Systems,* vol. 45, no. 10, pp. 1032-1042, 2017.

[77] R. W. A. A. De Doncker, D. M. Divan, and M. H. Kheraluwala, "A three-phase soft-switched high-power-density DC/DC converter for high-power applications," *IEEE Transactions on Industry Applications,* vol. 27, no. 1, pp. 63-73, 1991.

[78] S. Kenzelmann, A. Rufer, D. Dujic, F. Canales, and Y. R. de Novaes, "A versatile DC/DC converter based on modular multilevel converter for energy collection and distribution," pp. 71-71, 2011.

[79] D. Jovcic, "Step-up DC–DC converter for megawatt size applications," *IET Power Electronics,* vol. 2, no. 6, pp. 675-685, 2009.

[80] O. Abutbul, A. Gherlitz, Y. Berkovich, and A. Ioinovici, "Step-up switching-mode converter with high voltage gain using a switched-capacitor circuit," *IEEE Transactions on Circuits and Systems I: Fundamental Theory and Applications,* vol. 50, no. 8, pp. 1098-1102, 2003.

[81] D. Jovcic and L. Zhang, "LCL DC/DC Converter for DC Grids," *IEEE Transactions on Power Delivery,* vol. 28, no. 4, pp. 2071-2079, 2013.

[82] E. Veilleux, P. W. Lehn, and B.-T. Ooi, "Marx dc–dc converter for high-power application," *IET Power Electronics,* vol. 6, no. 9, pp. 1733-1741, 2013.

[83] J. A. Ferreira, "The Multilevel Modular DC Converter," *IEEE Transactions on Power Electronics,* vol. 28, no. 10, pp. 4460-4465, 2013.

[84] G. J. Kish, M. Ranjram, and P. W. Lehn, "A Modular Multilevel DC/DC Converter With Fault Blocking Capability for HVDC Interconnects," *IEEE Transactions on Power Electronics,* vol. 30, no. 1, pp. 148-162, 2015.

[85] M. Zhao, Z. Chen, and F. Blaabjerg, "Modeling of DC/DC Converter for DC Load Flow Calculation," pp. 561-566, 2006.

[86] S. Inoue and H. Akagi, "A Bidirectional DC–DC Converter for an Energy Storage System With Galvanic Isolation," *IEEE Transactions on Power Electronics,* vol. 22, no. 6, pp. 2299-2306, 2007.

[87] X. Yanhui, S. Jing, and J. S. Freudenberg, "Power Flow Characterization of a Bidirectional Galvanically Isolated High-Power DC/DC Converter Over a Wide Operating Range," *IEEE Transactions on Power Electronics,* vol. 25, no. 1, pp. 54-66, 2010.

[88] W. Chen, A. Q. Huang, C. Li, G. Wang, and W. Gu, "Analysis and Comparison of Medium Voltage High Power DC/DC Converters for Offshore Wind Energy Systems," *IEEE Transactions on Power Electronics,* vol. 28, no. 4, pp. 2014-2023, 2013.

[89] G. J. Kish, C. Holmes, and P. W. Lehn, "Dynamic modeling of modular multilevel DC/DC converters for HVDC systems," pp. 1-7, 2014.

[90] J. Zeng, W. Qiao, L. Qu, and Y. Jiao, "An Isolated Multiport DC–DC Converter for Simultaneous Power Management of Multiple Different Renewable Energy Sources," *IEEE Journal of Emerging and Selected Topics in Power Electronics,* vol. 2, no. 1, pp. 70-78, 2014.

[91] H. Wu, P. Xu, H. Hu, Z. Zhou, and Y. Xing, "Multiport Converters Based on Integration of Full-Bridge and Bidirectional DC–DC Topologies for Renewable Generation Systems," *IEEE Transactions on Industrial Electronics,* vol. 61, no. 2, pp. 856-869, 2014.

[92] Q. Zhijun, O. Abdel-Rahman, and I. Batarseh, "An Integrated Four-Port DC/DC Converter for Renewable Energy Applications," *IEEE Transactions on Power Electronics,* vol. 25, no. 7, pp. 1877-1887, 2010.

[93] S. Rezaee and E. Farjah, "A DC–DC Multiport Module for Integrating Plug-In Electric Vehicles in a Parking Lot: Topology and Operation," *IEEE Transactions on Power Electronics,* vol. 29, no. 11, pp. 5688-5695, 2014.

[94] Z. Ding, C. Yang, Z. Zhang, C. Wang, and S. Xie, "A Novel Soft-Switching Multiport Bidirectional DC–DC Converter for Hybrid Energy Storage System," *IEEE Transactions on Power Electronics,* vol. 29, no. 4, pp. 1595-1609, 2014.

[95] S. Falcones, R. Ayyanar, and X. Mao, "A DC–DC Multiport-Converter-Based Solid-State Transformer Integrating Distributed Generation and Storage," *IEEE Transactions on Power Electronics,* vol. 28, no. 5, pp. 2192-2203, 2013.

[96] Z. Wang and H. Li, "An Integrated Three-Port Bidirectional DC–DC Converter for PV Application on a DC Distribution System," *IEEE Transactions on Power Electronics,* vol. 28, no. 10, pp. 4612-4624, 2013.

[97] D. Jovcic and W. Lin, "Multiport High-Power LCL DC Hub for Use in DC Transmission Grids," *IEEE Transactions on Power Delivery,* vol. 29, no. 2, pp. 760-768, 2014.

[98] W. Lin, J. Wen, and S. Cheng, "Multiport DC–DC Autotransformer for Interconnecting Multiple High-Voltage DC Systems at Low Cost," *IEEE Transactions on Power Electronics,* vol. 30, no. 12, pp. 6648-6660, 2015.

[99] R. G.-R. H. Feyzi, M. Sabahi, S. Najafi-Ravadanegh, "Incorporating DC–DC Boost Converters in Power Flow Studies," *Journal of Power Technologies,* no. Vol 97, No 1 (2017), pp. 28–34, 2017.

[100] D. A. Braunagel, L. A. Kraft, and J. L. Whysong, "Inclusion of DC converter and transmission equations directly in a Newton power flow," *IEEE Transactions on Power Apparatus and Systems,* vol. 95, no. 1, pp. 76-88, 1976.

[101] S. Mousavizadeh, M. R. Haghifam, and M. H. Shariatkhah, "A new approach for load flow calculation in AC/DC distribution networks considering the control strategies of different converters," (in English), *International Transactions on Electrical Energy Systems,* vol. 26, no. 11, pp. 2479-2493, Nov 2016.

[102] Z. Z. X. L. Chen, P. Zi and X. X. Zhou, "VSC based DC grid power flow algorithm and AC/DC power flow algorithm," presented at the Power System Technology (POWERCON), Chengdu, China, 2014.

[103] N. Mohan and T. M. Undeland, *Power electronics: converters, applications, and design*. Wiley India, 2007.

[104] A. Yazdani and R. Iravani, *Voltage-Sourced Converters in Power Systems: Modeling, Control, and Applications*. Wiley, 2010.

[105] N. Flourentzou, V. G. Agelidis, and G. D. Demetriades, "VSC-Based HVDC Power Transmission Systems: An Overview," *IEEE Transactions on Power Electronics,* vol. 24, no. 3, pp. 592-602, 2009.

[106] S. Rudraraju, S. C. Srivastava, A. K. Srivastava, and N. N. Schulz, "Modeling and Simulation of Voltage Source Converter–Medium-voltage DC System for Stability Analysis," *Electric Power Components and Systems,* vol. 39, no. 11, pp. 1134-1150, 2011.

[107] Z. Yang, H. Zhong, A. Bose, Q. Xia, and C. Kang, "Optimal Power Flow in AC–DC Grids With Discrete Control Devices," *IEEE Transactions on Power Systems,* vol. 33, no. 2, pp. 1461-1472, 2018.

[108] A. Pizano-Martinez, C. R. Fuerte-Esquivel, H. Ambriz-Perez, and E. Acha, "Modeling of VSC-based HVDC systems for a Newton-Raphson OPF algorithm," (in English), *Ieee Transactions on Power Systems,* vol. 22, no. 4, pp. 1794-1803, Nov 2007.

[109] D. G. H. T. A. Lipo, *Pulse Width Modulation for Power Converters: Principles and Practice*. Wiley-IEEE Press, 2003.

[110] C. i. d. g. r. é. C. d. é. B4, *Guide for the Development of Models for HVDC Converters in a HVDC Grid*. CIGRÉ, 2014.

[111] C. Wang, X. Li, L. Guo, and Y. W. Li, "A Nonlinear-Disturbance-Observer-Based DC-Bus Voltage Control for a Hybrid AC/DC Microgrid," *IEEE Transactions on Power Electronics,* vol. 29, no. 11, pp. 6162-6177, 2014.

[112] L. Xiong, W. Peng, and L. Poh Chiang, "A Hybrid AC/DC Microgrid and Its Coordination Control," *IEEE Transactions on Smart Grid,* vol. 2, no. 2, pp. 278-286, 2011.

[113] A. Yazdani and R. Iravani, "A Unified Dynamic Model and Control for the Voltage-Sourced Converter Under Unbalanced Grid Conditions," *IEEE Transactions on Power Delivery,* vol. 21, no. 3, pp. 1620-1629, 2006.

[114] R. R. Sawant and M. C. Chandorkar, "A Multifunctional Four-Leg Grid-Connected Compensator," *IEEE Transactions on Industry Applications,* vol. 45, no. 1, pp. 249-259, 2009.

[115] C. Opathella and B. Venkatesh, "Three-Phase Unbalanced Power Flow Using aπ-Model of Controllable AC-DC Converters," *IEEE Transactions on Power Systems,* vol. 31, no. 6, pp. 4286-4296, 2016.

[116] W. Tinney and C. Hart, "Power Flow Solution by Newton's Method," *IEEE Transactions on Power Apparatus and Systems,* vol. PAS-86, no. 11, pp. 1449-1460, 1967.

[117] T. Ochi, Y. Nonaka, D. Yamashita, K. Koyanagi, and R. Yokoyama, "Reliable power flow calculation with improved convergence characteristics for distribution systems," *IEEE PES Innovative Smart Grid Technologies*, pp. 1-6, 2012.

[118] B. Stott and O. Alsac, "Fast Decoupled Load Flow," *IEEE Transactions on Power Apparatus and Systems*, vol. PAS-93, no. 3, pp. 859-869, 1974.

[119] W. H. Kersting, "Radial test feeders," in *Proc. IEEE PES Winter Meeting*, 2001, pp. 908–912.

[120] M. E. Baran and F. F. Wu, "Network Reconfiguration in Distribution-Systems for Loss Reduction and Load Balancing," (in English), *Ieee Transactions on Power Delivery*, vol. 4, no. 2, pp. 1401-1407, Apr 1989.

[121] J. Mahseredjian, "Load-Flow options (EMTP-EMTPWorks)," 2014.

APPENDIX A JACOBIAN MATRIX'S ELEMENTS IN DECOUPLED LOAD-FLOW METHOD

The Jacobian matrix's (equation (3.62)) elements of the decoupled load-flow method are stated in this appendix [37]. They are partial derivative of power mismatch equations (3.58)-(3-60) with respect to the unknown variables (AC bus voltage magnitude (V_{ac}) and phase angle (δ), DC bus voltage (V_{dc}), and the frequency of system (ω)). Subscripts "i" and "j" are used for AC buses, "m" and "l" for DC buses, and "c" for interlinking converter buses.

$$\frac{\partial P_{mis,i}^{ac}}{\partial V_{ac,i}} = -P_{L_0,i}\left[2\frac{Z_{p,i}}{\left(V_{ac_0,i}\right)^2}V_{ac,i} + \frac{I_{p,i}}{V_{ac_0,i}}\right]\left(1 + K_{pf,i}(\omega - \omega_0)\right) - 2V_{ac,i}G_{ii} - \sum_{\substack{j=1 \\ j\neq i}}^{N_{AC}} V_{ac,j}(G_{ij}\,cos(\delta_i - \delta_j) + B_{ij}\,sin(\delta_i - \delta_j)) \tag{A.1}$$

$$\frac{\partial P_{mis,i}^{ac}}{\partial \omega} = -1/\vartheta_{p_{ac},i} - P_{L_0,i}\left[Z_{p,i}\left(\frac{V_{ac,i}}{V_{ac_0,i}}\right)^2 + I_{p,i}\left(\frac{V_{ac,i}}{V_{ac_0,i}}\right) + P_{p,i}\right]K_{pf,i} - V_{ac,i}\sum_{j=1}^{N_{AC}} V_{ac,j}\left(\frac{\partial G_{ij}}{\partial \omega}\,cos(\delta_i - \delta_j) + \frac{\partial B_{ij}}{\partial \omega}sin(\delta_i - \delta_j)\right) \tag{A.2}$$

$$\frac{\partial P_{mis,c}^{ac}}{\partial \omega} = -1/\vartheta_{p_{ac},c} - \frac{2}{\vartheta_{IC,c}(\omega^{max} - \omega^{min})} - P_{L_0,c}\left[Z_{p,c}\left(\frac{V_{ac,c}}{V_{ac_0,c}}\right)^2 + I_{p,c}\left(\frac{V_{ac,c}}{V_{ac_0,c}}\right) + P_{p,c}\right]K_{pf,c} - V_{ac,c}\sum_{j=1}^{N_{AC}} V_{ac,j}\left(\frac{\partial G_{cj}}{\partial \omega}\,\cos(\delta_c - \delta_j) + \frac{\partial B_{cj}}{\partial \omega}\sin(\delta_c - \delta_j)\right) \tag{A.3}$$

$$\frac{\partial P_{mis,i}^{ac}}{\partial \delta_i} = V_{ac,i}\sum_{\substack{j=1 \\ j\neq \mathrm{i}}}^{N_{AC}} V_{ac,j}(-G_{ij}\sin(\delta_i - \delta_j) + B_{ij}\cos(\delta_i - \delta_j)) \tag{A.4}$$

$$\frac{\partial P_{mis,i}^{ac}}{\partial \delta_j} = V_{ac,i}V_{ac,j}\left(G_{ij}\sin(\delta_i - \delta_j) - B_{ij}\cos(\delta_i - \delta_j)\right),\ (j \neq \text{i}) \tag{A.5}$$

$$\frac{\partial P_{mis,i}^{ac}}{\partial V_{dc,m}} = 0 \tag{A.6}$$

$$\frac{\partial P_{mis,c}^{ac}}{\partial V_{dc,m}} = 0 \tag{A.7}$$

$$\frac{\partial P_{mis,i}^{ac}}{\partial V_{dc,c}} = 0 \tag{A.8}$$

$$\frac{\partial P_{mis,c}^{ac}}{\partial V_{dc,c}} = \frac{2}{\vartheta_{IC,c}(V_{dc,c}^{max} - V_{dc,c}^{min})} \tag{A.9}$$

$$\begin{aligned}\frac{\partial Q_{mis,i}^{ac}}{\partial V_{ac,i}} = &-1/\vartheta_{q_{ac},i} - Q_{L_0,i}\left[2\frac{Z_{q,i}}{\left(V_{ac_0,i}\right)^2}V_{ac,i} + \frac{I_{q,i}}{V_{ac_0,i}}\right]\left(1 + K_{qf,i}(\omega - \omega_0)\right) \\ &+ 2V_{ac,i}B_{ii} - \sum_{\substack{j=1 \\ j\neq i}}^{N_{AC}} V_{ac,j}\left(G_{ij}\,sin(\delta_i - \delta_j) - B_{ij}\,cos(\delta_i - \delta_j)\right)\end{aligned} \tag{A.10}$$

$$\begin{aligned}\frac{\partial Q_{mis,c}^{ac}}{\partial V_{ac,c}} = &-1/\vartheta_{q_{ac},c} + \begin{cases}-1/\vartheta_{qc,c}\ , P_{IC} > 0\ \ and\ \ 1/\vartheta_{qc,c}\left(V_{ac_0} - V_{ac}\right) > Q_{c\ lim,c} \\ 0 \qquad\qquad\qquad\qquad\qquad\qquad\qquad\qquad\qquad\qquad Otherwise\end{cases} \\ &- Q_{L_0,c}\left[2\frac{Z_{q,c}}{\left(V_{ac_0,c}\right)^2}V_{ac,c} + \frac{I_{q,c}}{V_{ac_0,c}}\right]\left(1 + K_{qf,c}(\omega - \omega_0)\right) + 2V_{ac,c}B_{cc} \\ &- \sum_{\substack{j=1 \\ j\neq i}}^{N_{AC}} V_{ac,j}\left(G_{cj}\,sin(\delta_c - \delta_j) - B_{cj}\,cos(\delta_c - \delta_j)\right)\end{aligned} \tag{A.11}$$

$$\begin{aligned}\frac{\partial Q_{mis,i}^{ac}}{\partial \omega} = &-Q_{L_0,i}\left[Z_{q,i}\left(\frac{V_{ac,i}}{V_{ac_0,i}}\right)^2 + I_{q,i}\left(\frac{V_{ac,i}}{V_{ac_0,i}}\right) + P_{q,i}\right]K_{qf,i} \\ &- V_{ac,c}\sum_{j=1}^{N_{AC}} V_{ac,j}\left(\frac{\partial G_{cj}}{\partial \omega}sin(\delta_c - \delta_j) - \frac{\partial B_{cj}}{\partial \omega}cos(\delta_c - \delta_j)\right)\end{aligned} \tag{A.12}$$

$$\frac{\partial Q_{mis,i}^{ac}}{\partial \delta_i} = V_{ac,i} \sum_{\substack{j=1 \\ j \neq i}}^{N_{AC}} V_{ac,j}(G_{ij}\, cos(\delta_i - \delta_j) + B_{ij}\, sin(\delta_i - \delta_j)) \tag{A.13}$$

$$\frac{\partial Q_{mis,i}^{ac}}{\partial \delta_j} = V_{ac,i} V_{ac,j}\left(-G_{ij}\, cos(\delta_i - \delta_j) - B_{ij}\, sin(\delta_i - \delta_j)\right) \text{ , } (j \neq \text{i}) \tag{A.14}$$

$$\frac{\partial Q_{mis,i}^{ac}}{\partial V_{dc,m}} = 0 \tag{A.15}$$

$$\frac{\partial P_{mis,m}^{dc}}{\partial V_{ac,i}} = 0 \tag{A.16}$$

$$\frac{\partial P_{mis,m}^{dc}}{\partial \omega} = 0 \tag{A.17}$$

$$\frac{\partial P_{mis,m}^{dc}}{\partial \delta_i} = 0 \tag{A.18}$$

$$\frac{\partial P_{mis,m}^{dc}}{\partial V_{dc,l}} = -V_{dc,m} G_{ml} \text{ , } (l \neq m) \tag{A.19}$$

APPENDIX B POWER BALANCE EQUATIONS IN GENERALIZED LOAD-FLOW METHOD

The equations for injected and calculated active and reactive powers at bus "i" (equations (3.64) and (3.65)) in generalized load-flow method are presented as follows [34]:

$$P_i^{inj} = \bar{W}_i\left(P_{ac,i}^G - P_{ac,i}^L + \eta_{i-i}P_{dc,i}^G - \eta_{i-r}^{-1}P_{dc,i}^L\right) + W_i\left(P_{dc,i}^G - P_{dc,i}^L + \eta_{i-r}P_{ac,i}^G - \eta_{i-r}^{-1}P_{ac,i}^L\right) \tag{B.1}$$

$$\begin{aligned} P_i^{cal} = \sum_{\substack{j=1 \\ j\neq i}}^{n} U_{ij}\Big[&\bar{W}_i\,\bar{W}_j\,\bar{D}_{ij}\left(V_i^2G_{ij} - V_iV_j\left(G_{ij}\,cos\left(\delta_i-\delta_j\right) + B_{ij}\,sin\left(\delta_i-\delta_j\right)\right)\right) \\ &+ \bar{W}_i\,\bar{W}_jD_{ij}\left(G_{dc,ij}\left(M_{ij}^{-2}V_i^2 - M_{ij}^{-1}V_iM_{ji}^{-1}V_j\right)\right)\left(a_1\eta_{ij-r}^{-1} + b_1\eta_{ij-i}\right) \\ &+ \bar{W}_i\,W_j\,D_{ij}\left(G_{dc,ij}\left(M_{ij}^{-2}V_i^2 - M_{ij}^{-1}V_iV_j\right)\right)\left(a_2\eta_{ij-r}^{-1} + b_2\eta_{ij-i}\right) \\ &+ W_i\,\bar{W}_j\,D_{ij}\left(G_{dc,ij}\left(V_i^2 - V_iM_{ji}^{-1}V_j\right)\right) + W_i\,W_j\,D_{ij}\left(G_{dc,ij}\left(V_i^2 - V_iV_j\right)\right)\Big] \end{aligned} \tag{B.2}$$

$$Q_i^{inj} = \bar{W}_i\left(Q_{ac,i}^G - Q_{ac,i}^L + Q_{dc-c,i}^G - Q_{dc-c,i}^L\right) \tag{B.3}$$

$$\begin{aligned} Q_i^{cal} = \sum_{\substack{j=1 \\ j\neq i}}^{n} U_{ij}\Big[&\bar{W}_i\,\bar{W}_j\,\bar{D}_{ij}\left(-V_i^2B_{ij} - V_iV_j\left(G_{ij}\,sin\left(\delta_i-\delta_j\right) - B_{ij}\,cos\left(\delta_i-\delta_j\right)\right)\right) \\ &+ \bar{W}_i\,\bar{W}_jD_{ij}P_{ij}\,tan\,\varphi_{c-ij} + \bar{W}_iW_j\,D_{ij}P_{ij}\,tan\,\varphi_{c-ij}\Big] \end{aligned} \tag{B.4}$$